

Star formation at very low metallicity. I: Chemistry and cooling at low densities

S. C. O. Glover^{1,2}, A.-K. Jappsen^{1,3}

¹*Astrophysikalisches Institut Potsdam,*

An der Sternwarte 16, 14482 Potsdam, Germany; sglover@aip.de

²*Department of Astrophysics, American Museum of Natural History,*

79th Street at Central Park West, New York, NY 10024-5192, USA

³*Canadian Institute for Theoretical Astrophysics,*

University of Toronto, 60 St. George Street, Toronto, ON M5S 3H8, Canada;

jappsen@cita.utoronto.ca

ABSTRACT

We present a simplified chemical and thermal model designed to allow computationally efficient study of the thermal evolution of metal-poor gas within large numerical simulations. Our main simplification is the neglect of the molecular chemistry of the heavy elements. The only molecular chemistry retained within the model is the formation and destruction of molecular hydrogen. Despite this major simplification, the model allows for accurate treatment of the thermal evolution of the gas within a large volume of parameter space. It is valid for temperatures $50 < T < 10000$ K and metallicities $0 < Z < 0.1 Z_{\odot}$. In gas with a metallicity $Z = 0.1 Z_{\odot}$, and in the absence of an incident ultraviolet radiation field, it is valid for hydrogen number densities $n_{\text{H}} \lesssim 500/t_{\text{char}} \text{ cm}^{-3}$, where t_{char} is the size in Myr of the characteristic physical timescale of interest in the problem. If $Z \ll 0.1 Z_{\odot}$, or if a strong ultraviolet radiation field is present, then the model remains accurate up to significantly higher densities. We also discuss some possible applications of this model.

Subject headings: astrochemistry — molecular processes — ISM: molecules — galaxies: formation – cosmology: theory

1. Introduction

It has long been known that cooling by molecular hydrogen, H_2 , plays a major role in regulating star formation in primordial protogalaxies (Saslaw & Zipoy 1967; Peebles & Dicke

1968; Matsuda et al. 1969; Lepp & Shull 1983; Tegmark et al. 1997; Abel et al. 2002). The importance of H_2 stems from the fact that in most circumstances it is the dominant coolant in primordial gas at $T < 10^4 \text{ K}$. As a result, the chemistry of H_2 in primordial gas has attracted considerable study (Dalgarno & Lepp 1987; Black 1991; Abel et al. 1997; Galli & Palla 1998; Stancil, Lepp, & Dalgarno 1998; Lepp, Stancil, & Dalgarno 2002) and it is now generally accepted that only a small chemical network, of maybe 20–30 reactions, is required to model H_2 chemistry over a very wide range of conditions in these systems.

The introduction of metals into the gas, as will occur following enrichment of their surroundings by the first generation of supernovae, complicates matters enormously. Many other atomic and molecular coolants become available and the associated chemistry is highly complex: for instance, a reasonably complex model of purely gas-phase chemistry can easily stretch to ~ 400 reactants and almost 4000 reactions (e.g. Le Teuff, Millar & Markwick 2000). This would not matter were it not for two important points. First, many astrophysicists believe that metal enrichment above a certain level – the so-called ‘critical metallicity’ – leads to a significant change in the stellar initial mass function (IMF), from an IMF dominated by massive stars to one that looks far more like the familiar Salpeter IMF of local star formation (Bromm et al. 2001; Schneider et al. 2002). Second, testing this idea numerically using three-dimensional hydrodynamical simulations requires us to model the chemistry of the gas, but the highly detailed chemical models mentioned above are impractical to use in high-resolution numerical simulations, owing to their high computational cost. This is a consequence of the fact that chemical rate equations are frequently stiff and so for reasons of stability must be solved implicitly, with a computational cost that scales as the cube of the number of chemical species involved.

It is therefore important to look for ways to simplify the chemistry without unduly compromising the accuracy of the resulting model. Major simplifications can be made if we make the reasonable assumption that the main coolants in low metallicity, high redshift gas will be similar to those in the local interstellar medium – which should be true provided that the abundance ratios of the various metals in low metallicity gas are not *too* unusual – and also if we restrict the range of physical conditions in which we are interested.

In this paper, we present a chemical model designed to model the chemistry of the major coolants in cool ($T \lesssim 10^4 \text{ K}$) low-metallicity gas at low gas densities. In the absence of ultraviolet radiation, and in gas with $Z = 0.1 Z_\odot$, our model is valid for atomic hydrogen number densities $n_{\text{H}} \lesssim 500/t_{\text{char}} \text{ cm}^{-3}$, where t_{char} is the size in Myr of the characteristic physical timescale of interest in the problem, corresponding to an overdensity of $\delta = 2.5 \times 10^9 t_{\text{char}}^{-1} (1+z)^{-3}$ with respect to the cosmological mean background density. At lower metallicities, or if a moderately strong UV field is present, our model remains accurate up to

significantly higher densities. We do not treat the cooling or chemistry of hot gas ($T \gg 10^4 \text{K}$) as this has already been treated in detail elsewhere (see e.g. Sutherland & Dopita 1993).

The structure of this paper is as follows. In §2 we present our simplified chemical network and discuss the principles determining our choice of reactants (§2.1) and reactions (§2.2), as well as our treatment of grain surface chemistry (§2.3) and photochemistry (§2.4). In §3, we discuss our treatment of the main thermal processes included in our model, with a particular emphasis on atomic fine structure cooling. We conclude in §4 with a brief discussion of possible applications of our model.

2. Chemical model

2.1. Choice of chemical species

Our choice of which chemical species to include in our simplified network was guided by two main considerations. In order to properly model the thermal evolution of the gas, we must be able to accurately model the evolution of the chemical abundances of all of the major coolants. At the same time, in order to keep our chemical treatment computationally efficient, we do not want to include more species than are strictly necessary. In some cases, the decision on whether or not to include a species was obvious. For instance, neutral atomic hydrogen, H, is a major constituent of the gas and is also a major coolant at $T \sim 10^4 \text{K}$ and above. Molecular hydrogen, H_2 , also must be included as it has long been recognised to be the dominant coolant in metal-free gas at $200 < T < 10^4 \text{K}$ (Saslaw & Zipoy 1967; Peebles & Dicke 1968), and it is now clear that it also remains significant in metal-poor gas (Omukai et al. 2005; Santoro & Shull 2006; Jappsen et al. 2007). A good case can also be made for the inclusion of HD, which dominates the cooling in zero-metallicity gas at $T < 200 \text{K}$ (Flower et al. 2000), and which remains important at least up to metallicities $Z \sim 10^{-5} Z_\odot$ (Omukai et al. 2005). As far as metals go, however, the choice is less obvious. Metal atoms and ions produce little in the way of resonance line cooling at $T < 10^4 \text{K}$, but many can act as sources of fine structure line emission or emission from metastable transitions at these temperatures. Therefore, in order to determine which of the various species are important coolants in the region of parameter space that our model is designed to cover, we directly compared the cooling rates produced by each species, under the assumption that the relative abundances of the various elements were the same as in the local interstellar medium.

The species we investigated in this comparison were the same as those included in the shock models of Hollenbach & McKee (1989): C, C^+ , Cl, Cl^+ , Fe, Fe^+ , N, N^+ , Ne^+ , Ni, Ni^+ ,

O, O⁺, S, S⁺, Si and Si⁺. This list includes all of the neutral or singly ionized species that have both non-negligible abundances and emission lines that are accessible at $T < 10^4$ K. Doubly ionized species are unlikely to be abundant in gas of this temperature, and so are unlikely to contribute significantly to the total cooling rate. Atomic data for C, C⁺, O, Si and Si⁺ was taken from the sources listed in Tables 5–6. For the remaining species, we used data taken from Hollenbach & McKee (1989). For the relative abundances of C, Fe, N, Ne, Ni, O, S and Si, we used values taken from Sembach et al. (2000), while for Cl we used a value taken from Asplund, Grevesse & Sauval (2006).

We investigated three different scenarios for the ionization state of the gas, which we here refer to as the ‘no ionization’, ‘moderate ionization’ and ‘high ionization’ cases. In the no ionization case, we assumed that the gas was completely neutral, and so set the electron abundance to zero, along with the abundances of all of the ionized species. In the moderate ionization case, we assumed that the fractional ionization of hydrogen was such that $n_{\text{H}^+}/n_{\text{H}} = 10^{-4}$, that species with ionization potentials lower than that of hydrogen – C, Cl, Fe, Ni, S and Si – were fully ionized, and that all of the other species remained fully neutral. Finally, in the high ionization case, we assumed that $n_{\text{H}^+}/n_{\text{H}} = 0.5$, that species with ionization potentials lower than that of hydrogen were again fully ionized, and that the fractional ionization of the other species was the same as that of hydrogen, i.e. 50%.

In each case, we computed the cooling rate due to fine structure and/or metastable transitions from each of the listed species for a large number of temperatures in the interval $50 < T < 10000$ K and number densities in the interval $0.001 < n < 100 \text{ cm}^{-3}$. In these calculations, we assumed that the total metallicity of the gas was $0.1 Z_{\odot}$, and that the gas was optically thin in all of the relevant transitions. We also calculated the contributions to the total cooling rate made by H I Lyman- α emission and Compton cooling; the rate of the latter was calculated for an assumed redshift $z = 20$.

We used the results of our comparison to select the set of major coolants that it was necessary to include in our thermal model by identifying all of the coolants that contributed more than 25% of the total cooling rate for any of the combinations of temperature, density and ionization that we examined. The resulting set consisted of C, C⁺, O, Si⁺, Compton cooling and Lyman- α cooling. Therefore, the only metals that we include in our chemical and thermal model are carbon, oxygen and silicon. The importance of carbon and oxygen is unsurprising – they are well known to play a major role in the cooling of the local atomic ISM (Wolfire *et al.* 2003), and previous authors have also predicted that they will play a key role at high redshift (see e.g. Bromm et al. 2001; Bromm & Loeb 2003; Santoro & Shull 2006; Frebel, Johnson & Bromm 2007). Silicon has attracted less attention (although see Santoro & Shull 2006), but Si⁺ proves to be the dominant coolant in highly ionized gas with

$700 \lesssim T \lesssim 7000$ K at $n > 0.3 \text{ cm}^{-3}$. Although gas with the very high fractional ionization assumed here will recombine quickly at temperatures $T < 10^4$ K, it nevertheless seems prudent to include silicon in our model. Moreover, since it is necessary to include neutral silicon in our chemical model if we are to calculate the Si^+ abundance accurately, it requires little extra effort to include the effects of fine-structure cooling from Si I .

Our choice of a 25% cutoff in this analysis is somewhat arbitrary. If we were to decrease the size of this cutoff, we would find that the number of species that must be included would increase, as both Fe^+ and S are important coolants at the 10–20% level in portions of our parameter space. However, as the cooling rates of the dominant coolants often have uncertainties that are comparable to or larger than the size of the contributions from these minor coolants, the accuracy we would gain by including them is less than might be expected, and does not (in our opinion) justify the additional complexity and computational expense that would be required in order to treat them.

Finally, it is clear that our conclusions here are sensitive to our choice of elemental abundance ratios. For instance, an increase in the iron abundance (relative to the other metals) of 1–2 orders of magnitude would render Fe and Fe^+ important coolants in portions of our parameter space, necessitating their inclusion in our model. Such an increase would be expected if the enrichment of the gas were dominated by pair-instability supernovae with masses close to the top end of the $140\text{--}260 M_\odot$ allowed mass range (Heger & Woosley 2002). However, studies of the abundance ratios found in extremely metal-poor stars in the Galactic halo, which at present give us the best picture available of the elemental composition of very metal-poor gas, do not find evidence for significant enrichment by pair-instability supernovae (see e.g. the discussion in Tumlinson, Venkatesan & Shull 2004) and so at the present time there is no compelling reason to include iron in our chemical model.

Our chemical model therefore consists of the eight coolants discussed above – H, H_2 , HD, C, C^+ , O, Si and Si^+ – together with ten additional species that play key roles in determining one or more of the abundances of the coolants: e^- , H^+ , H^- , H_2^+ , He, He^+ , D, D^+ , O^+ and Si^{++} . Our rationale for including He and He^+ in our model is that in the presence of a significant flux of hard UV photons, X-rays or cosmic rays, ionized helium can act as an important source of free electrons, and moreover can transfer charge to neutral carbon or silicon (but not oxygen) more far effectively than H^+ can.

We do not include minor primordial coolants such as LiH or H_3^+ . These are never important at low densities and rarely important at high densities (see Mizusawa, Omukai & Nishi 2005, Glover & Savin 2006, 2007). More significantly, we do not include molecular coolants such as CO or H_2O , assuming instead that the bulk of the carbon and oxygen in the gas remains in atomic or ionized form. This assumption dramatically simplifies the chemical

modelling of the gas, but at the same time restricts the range of physical conditions over which the resulting model is useful.

To assess the conditions for which this approximation is justified, we need to know two things. First, what fraction of the available carbon and oxygen must be locked up in CO or H₂O in order for cooling from these molecules to dominate over fine structure cooling? Second, under what conditions are these fractions achievable within a dynamically interesting timescale? To answer the first of these questions, we have performed calculations using the treatment of carbon and oxygen fine structure cooling discussed in §3.1 below, together with a table-based treatment of CO and H₂O taken from Neufeld & Kaufman (1993) and Neufeld, Lepp & Melnick (1995). We have computed f_{mol} , defined as

$$f_{\text{mol}} = \frac{\Lambda_{\text{CO}} + \Lambda_{\text{H}_2\text{O}}}{\Lambda_{\text{C}^+} + \Lambda_{\text{C}} + \Lambda_{\text{O}}}, \quad (1)$$

where Λ_i is the cooling rate per unit volume due to species i , for a wide range of temperatures and densities. We assume that $n_{\text{H}} \gg \max(n_{\text{H}_2}, n_{\text{e}})$ and that all of the cooling occurs in the optically thin regime. We adopt a nominal redshift $z = 20$ and consider only temperatures $T > T_{\text{CMB}}(z) = 57.2$ K, under the assumption that heating from the CMB will prevent the gas from cooling appreciably below this temperature. In Figure 1, we show how f_{mol} varies as a function of temperature and density.

Figure 1 demonstrates that over most of the parameter space that we have examined, f_{mol} is of order unity. We find that $f_{\text{mol}} > 10$ only for temperatures very close to the CMB temperature (which is likely an numerical artifact, a result of the fact that our treatment of fine structure cooling includes the effects of radiative pumping by the CMB, while our treatment of CO and H₂O cooling does not), and at high densities, where the level populations of the fine structure coolants start to reach their local thermodynamic equilibrium values, causing the fine structure cooling rate per atom to saturate. For CO or H₂O cooling to be effective, we therefore require that about as many carbon and oxygen atoms be incorporated into molecules as remain in atomic form.

With these values of f_{mol} in hand, we can now turn to the question of whether it is possible to produce enough CO and H₂O in the gas within an interesting timescale. Since we require a significant amount of oxygen to be in the form of coolant molecules, the timescale of interest, t_{conv} , is given approximately by

$$t_{\text{conv}} \simeq \frac{n_{\text{O}}}{R_{\text{f}}} \quad (2)$$

where R_{f} is the net rate of formation of coolants per unit volume. Therefore, to estimate t_{conv} we must first estimate R_{f} .

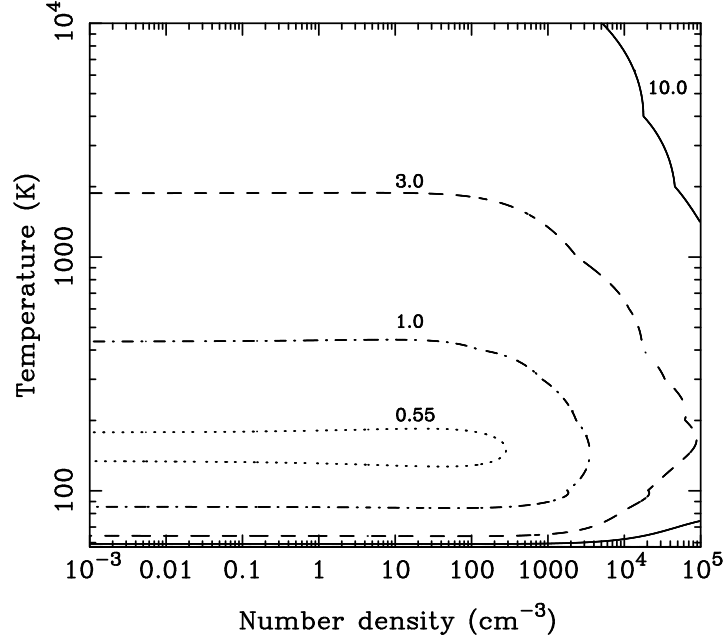
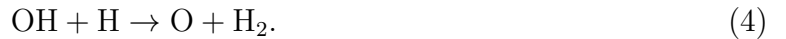


Fig. 1.— Value of f_{mol} (see Equation 1) as a function of temperature and density. Contours corresponding to $f_{\text{mol}} = 0.55$ (*dotted*), 1.0 (*dot-dashed*), 3.0 (*dashed*) and 10.0 (*solid*) are plotted. We see that $f_{\text{mol}} < 10$ for almost the whole of the parameter space considered.

Although a complete discussion of the formation and destruction mechanisms of CO and H₂O in low metallicity gas is beyond the scope of this paper, we will briefly summarize the most important points. In hot gas ($T \gtrsim 600$ K), most CO and water molecules form via reaction pathways initiated by the hydroxyl radical, OH (see e.g. Hollenbach & McKee 1979; Wagner & Graff 1987). This is formed by



but most is then destroyed by



However, a small fraction instead reacts to form other molecular species, such as water or CO, e.g.



The resulting H₂O and CO molecules can be destroyed by collisions with atomic hydrogen:



If, as will generally be the case in low-metallicity gas, $x_{\text{H}_2} \lesssim 0.1$ (where x_{H_2} is the fractional abundance of H_2 relative to the total number of hydrogen nuclei), then the destruction of water by reaction 7 is far more effective than its formation by reaction 5, and water will never account for more than a small fraction of the available oxygen. On the other hand, the CO formed by reaction 6 can potentially account for almost all of the available oxygen or carbon – whichever is present in the smaller amount – as the destruction of CO by reaction 8 is ineffective at $T < 5000\text{K}$. Therefore, the net rate of formation of coolant molecules (primarily CO) is given approximately by

$$R_{\text{f}} \simeq \frac{k_3 k_6 x_{\text{C}}}{k_4 x_{\text{H}} + k_6 x_{\text{C}}} n_{\text{O}} n_{\text{H}_2} \text{ cm}^{-3} \text{ s}^{-1}, \quad (9)$$

where k_i is the rate coefficient of reaction i , x_{H} and x_{C} are the fractional abundances of atomic hydrogen and atomic carbon, and n_{O} and n_{H_2} are the number densities of O and H_2 respectively. The timescale to convert significant quantities of oxygen to CO is then given approximately by

$$t_{\text{conv}} \simeq \frac{n_{\text{O}}}{R_{\text{f}}}, \quad (10)$$

$$= \frac{1}{n_{\text{H}_2}} \frac{k_4 x_{\text{H}} + k_6 x_{\text{C}}}{k_3 k_6 x_{\text{C}}}. \quad (11)$$

For $x_{\text{H}_2} = 10^{-3}$, which is a reasonable value for low metallicity gas if H_2 formation on dust is unimportant, this gives a timescale of approximately

$$t_{\text{conv}} \simeq \frac{100}{n} \frac{Z_{\odot}}{Z} \text{ Myr}, \quad (12)$$

where n is the number density of hydrogen nuclei, and where we have adopted the values for the various rate coefficients that are given in Le Teuff, Millar & Markwick (2000).

In cold gas, all of these reactions (except for reaction 6) are ineffective, and other processes dominate the formation of water and CO. A good summary of the relevant chemistry is given in Black & Dalgarno (1977). When $x_{\text{O}} + x_{\text{H}_2} \gtrsim 10^{-9} x_{\text{O}} x_{\text{H}}$, the most important mechanism involves the formation of the OH^+ ion via the rapid ion-neutral reaction



If $x_{\text{e}} > 1.6 \times 10^{-3} T^{1/2} x_{\text{H}_2}$, then most of the resulting OH^+ ions simply dissociatively recombine:



Otherwise, they can then react further with H_2 to give H_2O^+ and H_3O^+ , with dissociative recombination of the latter producing OH and water. CO formation follows through reaction 6. All of these reactions occur rapidly, and so the net rate of formation of coolant

molecules is given by the rate of formation of OH^+ multiplied by the fraction of OH^+ that is not destroyed by dissociative recombination, f_{dr} :

$$R_{\text{f}} \simeq k_{13}(1.0 - f_{\text{dr}})n_{\text{O}^+}n_{\text{H}_2}, \quad (15)$$

For $x_{\text{e}} = 1.6 \times 10^{-3} T^{1/2} x_{\text{H}_2}$, we have $f_{\text{dr}} = 0.5$, and hence $R_{\text{f}} = 0.5k_{13}n_{\text{O}^+}n_{\text{H}_2}$. In that case, the time required to convert most of the oxygen to OH^+ and thence to other molecules is

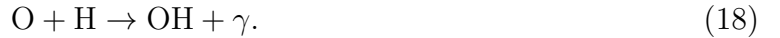
$$t_{\text{conv}} \simeq \frac{1}{k_{13}x_{\text{H}_2}x_{\text{H}^+}n}, \quad (16)$$

where we have used the fact that $n_{\text{O}^+}/n_{\text{O}} \simeq n_{\text{H}^+}/n_{\text{H}}$ owing to the rapid transfer of charge between oxygen and hydrogen (see §2.2.2 below). If we assume that $x_{\text{e}} \simeq x_{\text{H}^+}$ and that $x_{\text{H}_2} = 10^{-3}$, then this gives us a value for t_{conv} of

$$t_{\text{conv}} \simeq \frac{1000}{n} \text{ Myr}. \quad (17)$$

Decreasing the fractional ionization of the gas will increase t_{conv} , but increasing it will have no significant effect.

Finally, if the fractional ionization of the gas is too low for reaction 13 to operate effectively, then the formation of coolant molecules again occurs primarily via hydroxyl, which in this case is formed mainly by direct radiative association (Julienne, Krauss & Donn 1971; Smith & Zweibel 1976)



In this case, t_{conv} is simply

$$\begin{aligned} t_{\text{conv}} &= (k_{18}n)^{-1}, \\ &\simeq \frac{40}{n} \text{ Gyr}. \end{aligned} \quad (19)$$

Comparing the three values of t_{conv} derived above, we see that in gas with $Z = 0.1 Z_{\odot}$, $t_{\text{conv}} \simeq 1000n^{-1} \text{ Myr}$, regardless of the gas temperature, provided that $x_{\text{H}_2} \simeq 10^{-3}$ and that the fractional ionization satisfies the constraint given above. If we compare this with the characteristic physical timescale of the problem of interest, t_{char} , then it is simple to show that for densities

$$n \lesssim \frac{1000 \text{ Myr}}{t_{\text{char}}} \text{ cm}^{-3}, \quad (20)$$

CO and H_2O will not form in quantities large enough to dominate the cooling, and hence it is valid to ignore these molecules and all of their associated chemistry. Note also that if we were to include the effects of photodissociation of OH, H_2O and CO in the above analysis, then this would push the required density to an even larger value.

In a gravitationally collapsing protogalaxy, a reasonable value for t_{char} is the gravitational free-fall timescale t_{ff} , and in this scenario, our neglect of the molecular chemistry is valid as long as $n < 400 \text{ cm}^{-3}$. On the other hand, if we want to simulate the thermal evolution of the interstellar medium in a metal-poor dwarf galaxy, a more reasonable timescale may be the sound-crossing time of the disk, which is of order 100 Myr for a 1 kpc disk and a sound speed of 10 km s^{-1} . In this case, our model is valid only for $n < 10 \text{ cm}^{-3}$.

As a consistency check on our conclusions here, we examined the results of Omukai et al. (2005), who model the thermal and chemical evolution of freely-falling gas at a range of metallicities far below solar, using a detailed treatment of the gas chemistry. They find that for $Z = 0.01 Z_{\odot}$, significant conversion of carbon and oxygen to molecular form does not occur until $n > 10^3 \text{ cm}^{-3}$, in line with the value derived here. At lower metallicities, an even higher gas density is required. As another check, we have computed the evolution of the CO and H₂O abundances in the gas at the center of several of the simulated protogalactic halos discussed in Jappsen et al. (2007; hereafter paper II), using values for the density, temperature, H₂ abundance and H⁺ abundance taken from our simulations, and modelling the chemistry with the full UMIST99 chemical network (Le Teuff, Millar & Markwick 2000). We find that in most of these runs, our neglect of the molecular coolants is justified, as their abundances never become large enough for them to significantly affect the cooling. Our approximation begins to break down in the runs with $Z = 0.1 Z_{\odot}$, where about 10%–20% of the total carbon and oxygen are incorporated into CO and H₂O, which is just enough to affect the cooling at high temperatures and/or high densities. However, only in our runs with $Z = Z_{\odot}$ does it break down completely. Therefore, the use of our highly simplified chemical model would appear to be justified in low-density gas with $Z \leq 0.1 Z_{\odot}$.

We are thus left with a set of eighteen chemical species that must be modelled: e[−], H⁺, H, H[−], H₂⁺, H₂, D⁺, D, HD, He, He⁺, C, C⁺, O, O⁺, Si, Si⁺ and Si⁺⁺. The combined evolution of the abundances of these species is described by a chemical network consisting of 74 reactions: 47 collisional gas-phase reactions (summarized in Table 1), 12 photochemical gas-phase reactions (summarized in Table 2), 7 grain surface reactions (summarized in Table 3), and 8 reactions involving cosmic rays (summarized in Table 4). The abundances of these species are also constrained by seven conservation laws:

$$x_{\text{H}^+} + x_{\text{H}_2^+} + x_{\text{D}^+} + x_{\text{He}^+} + x_{\text{C}^+} + x_{\text{O}^+} + x_{\text{Si}^+} + x_{\text{Si}^{++}} = x_{\text{e}} + x_{\text{H}^-}, \quad (21)$$

$$x_{\text{H}^+} + x_{\text{H}} + x_{\text{H}^-} + 2x_{\text{H}_2^+} + 2x_{\text{H}_2} + x_{\text{HD}} = 1, \quad (22)$$

$$x_{\text{D}^+} + x_{\text{D}} + x_{\text{HD}} = x_{\text{D, tot}}, \quad (23)$$

$$x_{\text{He}^+} + x_{\text{He}} = x_{\text{He, tot}}, \quad (24)$$

$$x_{\text{C}} + x_{\text{C}^+} = x_{\text{C, tot}}, \quad (25)$$

$$x_{\text{O}} + x_{\text{O}^+} = x_{\text{O, tot}}, \quad (26)$$

$$x_{\text{Si}} + x_{\text{Si}^+} + x_{\text{Si}^{++}} = x_{\text{Si, tot}} \quad (27)$$

where x_i is the fractional abundance of chemical species i relative to the total abundance of hydrogen nuclei, and where $x_{\text{D, tot}}$, $x_{\text{He, tot}}$, $x_{\text{C, tot}}$, $x_{\text{O, tot}}$, and $x_{\text{Si, tot}}$ are the total abundances of deuterium, helium, carbon, oxygen and silicon, respectively. Furthermore, we assume in our modelling that H^- and H_2^+ are in chemical equilibrium, allowing us to write their abundances as:

$$x_{\text{H}^-} = \frac{k_1 x_{\text{H}} x_{\text{e}} n}{(k_2 x_{\text{H}} + k_5 x_{\text{H}^+} + k_{15} x_{\text{e}} + k_{16} x_{\text{H}} + k_{17} x_{\text{H}^+}) n + R_{51}}, \quad (28)$$

and

$$x_{\text{H}_2^+} = \frac{(k_3 x_{\text{H}} x_{\text{H}^+} + k_7 x_{\text{H}_2} x_{\text{H}^+} + k_{17} x_{\text{H}^-} x_{\text{H}^+}) n}{(k_4 x_{\text{H}} + k_6 x_{\text{e}}) n + R_{52}}, \quad (29)$$

where n is the number density of hydrogen nuclei. This assumption is generally justified in simulations of the cooling and gravitational collapse of gas in protogalactic halos, as the timescales on which H^- and H_2^+ reach chemical equilibrium are much shorter than the cooling or free-fall timescale. (For a more detailed discussion of this point, see Glover et al. 2006).

The constraints represented by equations 21–29 allow us to reduce the total number of chemical rate equations that must be solved to only nine. In practice, we generally choose to solve for the abundances of the ionized species (H^+ , D^+ , He^+ , C^+ , O^+ , Si^+ , Si^{++}), H_2 and HD , but alternative choices are possible and would not significantly alter the results obtained.

2.2. Selection of reactions

The number of chemical reactions that could be included in our chemical network is very large, despite the limited number of chemical species involved. Fortunately, many of these reactions have little or no impact on the evolution of the abundances of our main coolants and so the number of reactions that need to be included in our chemical network remains reasonably small.

We can divide the reactions that must be included into two subsets. The first subset consists of the reactions required to model the chemistry of hydrogen, helium and deuterium, including the formation and destruction of H_2 and HD (reactions 1–29, 48–55, 60–63, 67–70). The second subset consists of the reactions required to model the carbon, oxygen and silicon chemistry (reactions 30–47, 56–59, 64–66, 71–74).

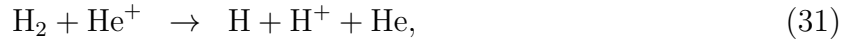
2.2.1. *Hydrogen, helium and deuterium chemistry*

The amount of H^+ present in the gas is controlled by seven main reactions: collisional ionization of H by electrons (reaction 11), charge transfer with helium (reactions 26 & 27), photoionization (reaction 48), cosmic ray ionization (reaction 67), gas-phase recombination (reaction 13) and recombination on the surface of dust grains (reaction 61). Similar reactions (nos. 12, 28, 29, 49, 68, 14 & 62) partially determine the D^+ abundance, but in this case, charge transfer to and from hydrogen (reactions 18 & 19) is also of great importance, owing to the very large abundance of hydrogen relative to deuterium. Finally, the He^+ abundance is controlled primarily by collisional ionization (reaction 24), photoionization (reaction 50), cosmic ray ionization (reaction 69), gas-phase and grain-surface recombination (reactions 25 & 63) and charge transfer with hydrogen (reactions 26 & 27).

The remaining 24 reactions in this subset control the formation and destruction of H_2 and HD. H_2 forms in the gas phase via the intermediate ions H^- and H_2^+ (reactions 2 & 4), as well as on the surface of dust grains (reaction 60). It is destroyed by collisions with H^+ , e^- , H and H_2 (reactions 7–10), and can also be photodissociated or photoionized by UV radiation (reactions 53 & 54), or ionized by cosmic rays (reaction 70). Collisions with He (Dove et al. 1987)



and He^+ (Barlow 1984)



can also destroy H_2 , but in general these processes are not as effective as collisions with hydrogen, and so they can be omitted from our simplified chemical model without significantly affecting its accuracy.

The H^- and H_2^+ ions required for gas-phase H_2 formation are formed primarily by the radiative association of atomic hydrogen with free electrons or protons respectively (reactions 1 & 3), and while reactions 2 & 4 generally dominate the removal of H^- and H_2^+ from the gas, in hot or highly ionized gas a number of other processes become competitive (reactions 5, 6 & 15–17). Photodissociation of H^- and H_2^+ (reactions 51 & 52) can also become important if the incident radiation field is strong.

Finally, although HD can form from intermediate ions such as D^- or HD^+ in a manner analogous to H_2 (see e.g. Stancil, Lepp, & Dalgarno 1998), most actually forms from H_2 via reaction 20:



The resulting HD can be destroyed by the inverse of this reaction (reaction 21), or by photodissociation (reaction 55). In hot gas, the HD abundance is also influenced by reactions between H_2 and D and HD and H (nos. 22 & 23 respectively). Note that with the exception of the grain surface reactions (which are discussed in §2.3 below), the reactions required to model the hydrogen, helium and deuterium chemistry accurately in metal-enriched gas are just the same as those required to model primordial gas.

The values for many of these rate coefficients are known to within a small amount of uncertainty at the temperatures and densities of interest, and so our choice of the particular values used here should be uncontroversial. However, a few of our assumptions demand further comment.

First, we note that the rates listed for reactions involving H_2 or HD as a reactant generally assume that these molecules are not vibrationally excited. This assumption is reasonable at the low densities treated here, but breaks down at densities $n \gtrsim 10^4 \text{ cm}^{-3}$.

Second, we note that for several reactions involving deuterium where no readily available rate coefficient exists in the astrophysical literature, we have assumed that the rate is the same as for the analogous reaction involving H or H^+ .

The rates of processes involving cosmic rays (see Table 4) depend on the energy spectrum and energy density of cosmic rays. These are poorly known at the relevant energies even in the local ISM, and far less is known concerning high-redshift cosmic rays. For this reason, we do not give absolute values for these rates, but instead parameterize them in terms of the cosmic ray ionization rate for atomic hydrogen, ζ_{H} , which can then be considered an adjustable parameter of the model.

Finally, we note that two of the reactions that regulate the H^- abundance have large uncertainties in their rate coefficients. The reactions in question are the associative detachment of H^- with H (reaction 2) and the mutual neutralization of H^- with H^+ (reaction 5). As discussed in Glover et al. (2006), the uncertainties in the rates of both of these reactions may be as large as an order of magnitude. In gas with a high fractional ionization, this uncertainty can lead to a significant uncertainty in the H_2 formation rate and in the final H_2 fractional abundance, particularly in the presence of a strong ultraviolet background radiation field. In the chemical model presented here, we have followed Galli & Palla (1998) and have adopted a rate coefficient for reaction 2 taken from Launay et al. (1991) and a rate coefficient for reaction 5 taken from Moseley et al. (1970). However, we caution the reader that this should not be regarded as an endorsement of the accuracy of these particular values.

2.2.2. Carbon, oxygen and silicon chemistry

As discussed in §2.1 above, we do not include the molecular chemistry of these elements in this simplified model. Our treatment of the carbon, oxygen and silicon chemistry is therefore purely a treatment of the charge balance of these species.

We begin with oxygen, in many respects the simplest of the three to treat. The ionization potential of neutral oxygen is only 0.02 eV larger than that of neutral hydrogen, and so charge transfer between O^+ and H or H^+ and O (reactions 36 & 37) occurs rapidly. Since the hydrogen abundance is orders of magnitude larger than the oxygen abundance, this means that the ratio of ionized to neutral oxygen is controlled by the ratio of ionized to neutral hydrogen, i.e. that

$$\frac{x_{O^+}}{x_O} \simeq \frac{k_{37}}{k_{36}} \frac{x_{H^+}}{x_H}. \quad (34)$$

In most circumstances, reactions 36 & 37 are the only reactions required in order to accurately model the oxygen chemistry. Nevertheless, for completeness we also include several other processes: radiative recombination (reaction 32), grain surface recombination (reaction 65), collisional ionization (reaction 35), charge transfer with He^+ (reaction 38), photoionization (reaction 57) and cosmic ray ionization (reaction 72).

In the case of carbon, the situation is rather different. First, charge transfer from H^+ to C (reaction 39) is much less effective than charge transfer from H^+ to O, and so reaction 39 plays a far less important role in the carbon chemistry than reaction 37 does in the oxygen chemistry. Second, carbon has an ionization potential of only 11.26 eV. This means that charge transfer from C^+ to H is significantly endothermic, rendering it unimportant at $T < 10^4$ K (although we include it here for completeness). It also means that neutral carbon can be photoionized by ultraviolet photons with wavelengths $\lambda > 912$ Å, which can penetrate easily into low metallicity protogalactic gas. Consequently, photoionization of C (reaction 56) plays an important role in the carbon chemistry, whereas photoionization of O^+ is unimportant outside of H II regions. In addition to charge transfer and photoionization, ionized carbon can also be produced by collisional ionization (reaction 33), although this is important only for temperatures $T > 9000$ K, by charge transfer with He^+ (reaction 41) and by cosmic ray ionization (reaction 71). C^+ is removed from the gas primarily by recombination in the gas phase (reaction 30) and on grain surfaces (reaction 64), although if the free electron abundance is small, charge transfer from C^+ to Si (reaction 44) can also become important.

In the case of silicon, a similar set of processes operate: collisional ionization (reaction 34), cosmic ray ionization (reaction 73), gas-phase recombination (reaction 31), grain surface recombination (reaction 66), charge transfer from H^+ , He^+ or C^+ to Si (reactions 42, 43 &

44), and photoionization by an ultraviolet radiation field (reaction 58), assuming one is present. In the case of silicon, however, we also include the doubly ionized ion, Si^{++} , in our chemical model, since this can be produced by charge transfer from H^+ to Si^+ (reaction 45) with an endothermicity of only a few eV, rendering it potentially important at temperatures $\sim 10^4$ K. It can also be produced by photoionization (reaction 59), although in this case the 16.35 eV energy requirement renders this process important only within H II regions, or by cosmic ray ionization (reaction 74). The Si^{++} produced by these processes can be destroyed by charge transfer with neutral hydrogen (reaction 46), or by recombination (reaction 47).

Regarding the accuracy of our adopted reaction rates, we note that while many have well determined rate coefficients, there are two notable exceptions. The only available rate coefficients for reactions 43 and 44, which involve the transfer of charge from He^+ to Si and from C^+ to Si respectively, assume that the reactions both proceed at the Langevin rate. In practice, highly exothermic charge transfer reactions often proceed at a rate far below the simple Langevin rate, and so the rates of these reactions may be overestimated in our model.

2.3. Grain surface chemistry

If dust grains are present in the metal-enriched gas, then our chemical model must account for the effects of reactions occurring on the surface of the grains, as these reactions are often far more effective than their gas-phase counterparts. We therefore include a small number of grain surface reactions in our model, as summarized in Table 3.

The only grain surface reaction between neutral species that is included in our model is the formation of molecular hydrogen (reaction 60). This is a hugely important reaction in the local interstellar medium, since at typical interstellar densities it is the only process capable of producing the large quantities of molecular hydrogen that are directly observed (see e.g. Wakker 2006) or inferred from other molecular tracers, such as CO. Theoretical modeling (Hirashita & Ferrara 2002; Glover 2003; Cazaux & Spaans 2004) suggests that it remains important down to metallicities of order $10^{-3} Z_{\odot}$, within the range of applicability for the chemical model presented here.

The rate that we adopt for this process is based on the widely used rate of Hollenbach & McKee (1989). This was derived for solar metallicity gas, assuming a distribution of grain sizes as given in Mathis, Rumpl & Nordsieck (1977), and to adapt it for use in low metallicity gas, we simply assume that the rate scales linearly with the metallicity Z . The validity of this assumption is open to question, as many of the features of the grain population, such as the grain size distribution or the mix of compositions, may differ greatly between Milky Way dust

and protogalactic dust. An alternative, physically motivated approach would be to adopt a grain size distribution and mix of compositions based on the results of numerical modeling of dust formation in high redshift supernovae (Todini & Ferrara 2001; Nozawa et al. 2003; Schneider, Ferrara & Salvaterra 2004) and then to compute the H_2 formation rate expected for this grain population. This is the approach used by Schneider et al. (2006). However, the uncertainties associated with this approach are considerable. To begin with, the predictions of the numerical models are highly sensitive to the degree of mixing assumed to occur within the supernova ejecta (Nozawa et al. 2003). In addition, dust destruction in the reverse shock is typically not taken into account in these models, and to the best of our knowledge, the amount of dust that survives the passage of the shock has yet to be fully quantified (although research in this area is actively proceeding; R. Schneider, priv. comm.). Finally, the changes wrought on the grain population by subsequent processing in the interstellar medium or intergalactic medium (see e.g. Venkatesan, Nath & Shull 2006) are not fully understood. In light of these uncertainties, we do not believe that this approach currently offers much of an advantage over our simple assumption of an H_2 formation rate that scales with metallicity.

We do not include any neutral-neutral surface reactions in our model other than H_2 formation. For neutral-neutral surface reactions to be able to significantly affect the ability of the gas to cool, they must be able to alter the abundances of neutral carbon, oxygen or silicon by a substantial amount. We can place an upper limit on the rate at which these reactions occur if we assume that the reaction probability $f_{\text{react}} = 1$, i.e. that every collision between a metal atom and a grain results in a reaction. In that case, the reaction rate per unit volume for an atomic species i is given by

$$R_i = v_{\text{th},i} A n_i, \quad (35)$$

where $v_{\text{th},i}$ is the thermal velocity of atomic species i , and A is the total surface area of grains per unit volume of gas. For Milky Way dust of the type assumed by Hollenbach & McKee (1989), $A \simeq 3 \times 10^{-21} n \text{ cm}^{-1}$, where n is the number density of hydrogen nuclei. At lower metallicity, our assumption that the grain size distribution does not change with metallicity implies that the value of A in gas with a metallicity Z is simply $A \simeq 3 \times 10^{-21} (Z/Z_\odot) n \text{ cm}^{-1}$. We can therefore rewrite equation 35 as

$$R_i \simeq 4.7 \times 10^{-17} \left(\frac{T}{m_i} \right)^{1/2} \left(\frac{Z}{Z_\odot} \right) n n_i, \quad (36)$$

where m_i is the mass of species i in atomic mass units. The corresponding conversion timescale $t_{\text{conv}} = n_i/R_i$ is then

$$t_{\text{conv}} = 2.1 \times 10^{16} n^{-1} \left(\frac{T}{m_i} \right)^{-1/2} \left(\frac{Z}{Z_\odot} \right)^{-1} \text{ s}. \quad (37)$$

If $f_{\text{react}} < 1$, then this expression becomes:

$$t_{\text{conv}} = 2.1 \times 10^{16} f_{\text{react}}^{-1} n^{-1} \left(\frac{T}{m_i} \right)^{-1/2} \left(\frac{Z}{Z_{\odot}} \right)^{-1} \text{ s.} \quad (38)$$

If we equate this to a characteristic physical timescale t_{char} , then we can show that $t_{\text{conv}} > t_{\text{char}}$ as long as

$$n < 665 \left(\frac{1 \text{ Myr}}{t_{\text{char}}} \right) f_{\text{react}}^{-1} \left(\frac{T}{m_i} \right)^{-1/2} \left(\frac{Z}{Z_{\odot}} \right)^{-1} \text{ cm}^{-3}. \quad (39)$$

For gas with a temperature $T = 2000 \text{ K}$ and metallicity $Z = 0.1 Z_{\odot}$, and with atomic carbon as the colliding species, this gives:

$$n < \frac{500 f_{\text{react}}^{-1} \text{ Myr}}{t_{\text{char}}} \text{ cm}^{-3}. \quad (40)$$

At higher temperatures, the limiting n will be slightly smaller, but at $T > 2000 \text{ K}$, collisional dissociation of most molecular species is highly effective, and so in this temperature regime, grain surface reactions are unlikely to be important.

From this analysis, we see that even if $f_{\text{react}} = 1$, neutral-neutral grain surface reactions are unimportant at gas densities $n < (500 \text{ Myr}/t_{\text{char}})(Z/0.1 Z_{\odot})^{-1} \text{ cm}^{-3}$. In gravitationally collapsing gas with $t_{\text{char}} = t_{\text{ff}}$, this corresponds to $n \lesssim 100(Z/0.1 Z_{\odot})^{-1} \text{ cm}^{-3}$. Note that a key point here is that for neutral-neutral grain surface reactions involving our atomic coolants (C, O etc.) to significantly affect the thermal behaviour of the gas, a large fraction of the total number of coolant atoms must react, whereas for grain surface reactions to affect the H_2 cooling rate by significantly altering the H_2 abundance, only a small fraction of the total number of hydrogen atoms must react. This means that in the case of H_2 , the relevant conversion timescale is several orders of magnitude shorter, and hence our density limit would be significantly smaller if we were to omit grain surface H_2 formation from our model.

One way in which this simple analysis could break down is if f_{react} were much larger for reactions involving the coolant atoms than for H_2 formation. However, a recent analysis of H_2 formation on grain surfaces by Cazaux & Tielens (2004) that takes both physisorbed (i.e. van der Waals bonded) and chemisorbed (i.e. chemically bonded) hydrogen into account demonstrates that in the conditions of interest in this paper, $f_{\text{react}} \sim 1$ (with the result that the computed H_2 formation rate is very similar to the widely-used rate of Hollenbach & McKee (1989) that is used in our model). A comparable analysis has not been performed for reactions involving C, O or Si, but clearly they cannot have $f_{\text{react}} > 1$, and so there is little scope for these reactions to occur significantly faster than H_2 formation.

Finally, we include in our surface chemistry model six important reactions involving ions: the recombination of H^+ , D^+ , He^+ , C^+ , O^+ and Si^+ with electrons on the surface of

grains. As grain surface recombination is a non-radiative process, it proceeds at a much faster rate than radiative recombination in the gas phase. Moreover, if a typical grain is negatively charged, then the effective cross-section for collisions will be much enhanced over the geometric cross-section due to Coloumb focussing. Grain charging is largely determined by the parameter (Bakes & Tielens 1994)

$$\psi = \frac{G\sqrt{T}}{n_e}, \quad (41)$$

where $G \simeq 0.01J_{21}$ is a measure of the radiation energy density between 6 eV and 13.6 eV relative to the Habing (1968) field. When ψ is small, most grains are negatively charged, and so in these conditions grain surface recombination can be important even if neutral-neutral grain surface reactions are unimportant.

To model grain surface recombination, we follow Weingartner & Draine (2001a). We adopt their rate coefficients for the recombination of H^+ , He^+ , C^+ and Si^+ . For O^+ and D^+ , we use the facts that O^+ and D^+ have almost the same ionization potential as H^+ and that the ion arrival rate at the grain scales as $m_i^{-1/2}$ (where m_i is the mass of the ion in atomic mass units) to derive rates by appropriately scaling the H^+ rate. The Weingartner & Draine rates were all computed for Milky Way dust, and to adapt them for use in low metallicity gas, we again assume that they scale linearly with Z , with the same caveats as before.

2.4. Photochemical rates

In Table 2, we list the cross-sections for all but two of the photochemical reactions included in our model. The two exceptions are H_2 photodissociation and HD photodissociation, which are caused by absorption in a large number of discrete spectral lines, and which are discussed separately in §2.4.1 below.

Given the cross-section, $\sigma(E)$, the corresponding photochemical rate can be obtained from

$$R_{\text{photo}} = 4\pi \int_{E_0}^{\infty} \frac{\sigma(E)I(E)}{E} e^{-\tau(E)} [1 + f(E)] dE \quad (42)$$

where E is the photon energy, E_0 is the energy threshold, $I(E)$ and $\tau(E)$ are the mean intensity (in units of $\text{eV s}^{-1} \text{cm}^{-2} \text{eV}^{-1} \text{sr}^{-1}$) and optical depth for a photon of energy E (both of which are problem dependent), and where $f(E)$ is a factor that accounts for the effects of secondary ionizations. It is generally a reasonable approximation to set $f(E) = 0$ unless the ionizing component of the radiation field is dominated by X-rays (Abel et al. 1997; Glover & Brand 2003). In the case that X-rays dominate, fits for $f(E)$ for H and

He photoionization as a function of the fractional ionization of the gas can be found in Shull & van Steenberg (1985) and Dalgarno, Yan & Liu (1999). The effects of secondary ionizations on the other processes listed here are generally negligible, owing to the large abundances of neutral H and He relative to all other species.

If the gas is optically thick at the He photoionization threshold, then an additional process that must be taken into account is the photoionization of H by the diffuse emission produced by He^+ recombination. In the limit of high optical depth, the on-the-spot approximation applies, and we can model this process as a local ionization rate with a value (Osterbrock 1989)

$$R_{\text{pi}} = [yk_{25,\text{rr,A}} + (0.96 - y)k_{25,\text{rr,B}} + k_{25,\text{di}}] n_e n_{\text{He}^+} \text{ cm}^{-3} \text{ s}^{-1}, \quad (43)$$

where y is given by

$$y = \frac{n_{\text{H}} \sigma_{48}(E_{\text{th,He}})}{n_{\text{H}} \sigma_{48}(E_{\text{th,He}}) + n_{\text{He}} \sigma_{50}(E_{\text{th,He}})}, \quad (44)$$

where $E_{\text{th,He}} = 24.6 \text{ eV}$ is the He ionization threshold. (Note that if $n_{\text{He}}/n_{\text{H}} \simeq 0.08$, as is the case in primordial gas with a low fractional ionization and low H_2 abundance, then $y \simeq 0.68$). If the on-the-spot approximation does not apply, then the radiative transfer of this diffuse emission must be modelled in some fashion. However, a discussion of appropriate techniques for doing so lies well beyond the scope of this paper.

In some circumstances it may also be necessary to take account of the photodissociation of H^- and H_2^+ by photons produced by ionized hydrogen and helium (both recombination emission and bremsstrahlung). This process is generally important only in neutral gas close to a significant volume of dense, ionized gas (e.g. in the neutral gas immediately surrounding an expanding ionization front). It is discussed in detail in Glover (2007) and so we do not discuss it further here.

Finally, we note that for each of the photoionization or photodissociation rates listed in Table 2, there is a corresponding photoheating rate, given by

$$R_{\text{heat}} = 4\pi \int_{E_0}^{\infty} \frac{\sigma(E)I(E)}{E} e^{-\tau(E)} (E - E_0) \eta(E - E_0) dE. \quad (45)$$

where $E - E_0$ is the energy of the primary photoelectron and $\eta(E - E_0) \leq 1$ gives the fraction of this energy converted to heat, which can be calculated using the results of Shull & van Steenberg (1985) or Dalgarno, Yan & Liu (1999). In practice, photoheating from the photoionization of H and He usually dominates over the other contributions by a wide margin.

2.4.1. H_2 and HD photodissociation

Although the binding energy of H_2 is only 4.48 eV, photons of this energy are not able to dissociate H_2 effectively, as the simplest dissociative transition – excitation to the vibrational continuum of the ground state – is strongly forbidden (Field, Somerville & Dressler 1966). Transitions to the repulsive $\text{b}^3\Sigma_u^+$ state, the least energetic of the excited electronic states of H_2 , are also forbidden, and so photodissociation takes place primarily through excitation to the Lyman ($\text{B}^1\Sigma_u^+$) or Werner ($\text{C}^1\Pi_u$) electronic states followed by radiative decay to the vibrational continuum of the ground state. As a number of vibrational levels are accessible in each excited state, photodissociation takes place through a number of discrete absorption lines, known as the Lyman and Werner band systems (Stecher & Williams 1967).

In optically thin gas, the photodissociation rate can be written as

$$R_{\text{diss}} = \sum_{v,J} R_{\text{diss},v,J} f_{v,J} \quad (46)$$

where $f_{v,J}$ is the fraction of H_2 molecules that have vibrational and rotational quantum numbers (v, J) in the electronic ground state, and $R_{\text{diss},v,J}$ is the photodissociation rate due to transitions out of (v, J) . The latter can be written as

$$R_{\text{diss},v,J} = \sum_{v',J'} \zeta_{v,J,v',J'} f_{\text{diss},v',J'}, \quad (47)$$

where $\zeta_{v,J,v',J'}$ is the pumping rate from level (v, J) in the electronic ground state to level (v', J') in either the Lyman or Werner states, $f_{\text{diss},v',J'}$ is the fraction of decays from v', J' which end in the vibrational continuum of the ground state (rather than back in some bound state), and where we sum over all accessible levels. Given appropriate molecular data, it is straightforward to calculate $R_{\text{diss},v,J}$ for each bound level (v, J) in the electronic ground state. To then calculate R_{diss} , one also needs to know the level populations $f_{v,J}$.

If we assume that the mean intensity $I(\nu) \equiv hI(E)$ is independent of energy, and that all of the H_2 is in the $v = 0, J = 0$ level (i.e. the para-hydrogen ground state), then R_{diss} evaluates to

$$R_{\text{diss}} = 1.38 \times 10^9 I(\nu) \text{ s}^{-1}, \quad (48)$$

where we have made use of molecular data taken from Abgrall et al. (1993a,b) and Abgrall, Roueff & Drira (2000). This expression remains a good approximation in the more general case that $I(\nu)$ is allowed to vary with frequency, provided that the variations are not too extreme and that we replace $I(\nu)$ in equation 48 with $I(\bar{\nu})$, where $h\bar{\nu} = 12.87 \text{ eV}$ (Abel et al. 1997):

$$R_{\text{diss}} = 1.38 \times 10^9 I(\bar{\nu}) \text{ s}^{-1}. \quad (49)$$

Relaxing the assumption that all of the H_2 has $J = 0$ also makes little difference to R_{diss} (Glover 2001). Vibrational excitation of the H_2 makes a much larger difference (Shull 1978), but at low gas densities we would expect the populations of the vibrational levels of H_2 to be very small. Equation 49 therefore gives a reasonable estimate of the optically thin H_2 photodissociation rate within the regions of parameter space for which our chemical model is valid.

If enough H_2 is present in the gas, then the Lyman-Werner lines can become optically thick, leading to a reduction in the H_2 photodissociation rate, an effect known as H_2 self-shielding. If the gas is at rest, then the effects of H_2 self-shielding can be treated quite accurately using the prescription of Draine & Bertoldi (1996). They parameterize the self-shielding with a shielding function f_{sh} , defined to be the ratio of the H_2 photodissociation rate in self-shielded gas to the rate in optically thin gas. They demonstrate how to calculate f_{sh} as a function of the gas temperature and the H_2 column density and also construct the following useful fitting function:

$$f_{\text{sh}} = \frac{0.965}{(1 + x/b_5)^2} + \frac{0.035}{(1 + x)^{1/2}} \exp \left[-8.5 \times 10^{-4} (1 + x)^{1/2} \right], \quad (50)$$

where $x = N_{\text{H}_2}/5 \times 10^{14} \text{ cm}^{-2}$, N_{H_2} is the H_2 column density, $b_5 = b/10^5 \text{ cm s}^{-1}$ and b is the Doppler broadening parameter. Although Draine & Bertoldi (1996) assume a semi-infinite slab geometry in their models, their approach is easy to extend to more complicated geometries.

Unfortunately, their simple treatment breaks down in gas which is not at rest. Doppler shifts due to the motions of the gas cause H_2 in different regions to absorb at slightly different wavelengths, and if these Doppler shifts are comparable to or larger than the thermal linewidth of the gas (as will be the case in transonic or supersonic gas respectively), then the effect is to reduce the amount of self-shielding that occurs. An accurate treatment of H_2 self-shielding in this regime probably requires one to solve the full frequency-dependent transport equation, which cannot currently be done in a computationally efficient manner within a three-dimensional hydrodynamics code. Consequently, various different approximations have been used to study H_2 photodissociation in this regime.

The simplest approach is to ignore self-shielding entirely (see e.g. Machacek et al. 2001, 2003). This is a good approximation if the velocities in the gas are large and the H_2 column densities are small, but otherwise will significantly overestimate the photodissociation rate. At the other extreme, one can ignore the effects of Doppler shifts (e.g. Yoshida et al. 2003; Hosokawa & Inutsuka 2006). This is a good approximation if the H_2 column density is sufficiently large ($N_{\text{H}_2} > 10^{19} \text{ cm}^{-2}$) that the Lorentz wings of the Lyman-Werner line profiles dominate the line widths, as in this case the line widths will be much larger than any likely

Doppler shifts within the molecular gas. On the other hand, this approach will underestimate the true photodissociation rate when $N_{\text{H}_2} < 10^{19} \text{ cm}^{-2}$, as is the case in many interesting low-metallicity systems.

Another approximation has recently been suggested by Ahn & Shapiro (2007). They use equation (50) to compute f_{sh} , but adopt a value for b that includes both a thermal contribution and one arising due to the velocity dispersion of the gas. In practice, this means that they treat their H_2 as having an effective b equivalent to that in a purely thermal gas with $T = 10^4 \text{ K}$. The accuracy of this approximation depends on the correlation length of the velocity field. If this is small compared to the other length scales of interest, then treating the velocity dispersion in this fashion is reasonable and should give a fairly accurate result. On the other hand, if the velocity field is dominated by large-scale bulk motions (such as infall into a protogalaxy), then this approximation will be significantly less accurate.

Finally, in Glover et al. (2006) and in paper II, we use a local approximation in which only the H_2 within a single SPH smoothing length is assumed to contribute to the shielding (see also Glover & Mac Low 2007a,b, for a grid-based version of this approach). This fairly crude approximation is intended to take account of the fact that H_2 close to a given point of interest is more likely to have only a small relative velocity than gas a large distance away. It will generally underestimate the amount of self-shielding, but nevertheless represents an improvement over neglecting self-shielding entirely. Aside from its inevitable inaccuracy, this approximation also suffers from the disadvantage of being resolution dependent, as increasing the number of SPH particles in the simulation will generally decrease all of the SPH smoothing lengths and hence will cause a systematic increase in f_{sh} . On the other hand, it has the significant advantages of being computationally efficient (as only local data is required) as well as being very easy to implement.

To sum up, a number of different approximate methods exist for treating H_2 self-shielding in large numerical simulations, but none are entirely satisfying. Further work on this problem is definitely called for.

Turning now to HD, we note that HD photodissociation in optically thin gas can be treated in much the same way as H_2 photodissociation. The necessary molecular data for HD can be found in Abgrall & Roueff (2006), and the resulting photodissociation rate for a radiation field with a flat spectrum can be written as

$$R_{\text{diss,HD}} = 1.5 \times 10^9 I(\nu) \text{ s}^{-1}, \quad (51)$$

which is only $\sim 10\%$ larger than the H_2 rate. Above an HD column density $N_{\text{HD}} \simeq 10^{13} \text{ cm}^{-2}$, self-shielding of the HD lines significantly reduces the photodissociation rate. For a static gas, this process can again be modeled using the approach of Draine & Bertoldi (1996), although

the same problems arise when one tries to extend this approach to a gas distribution which is not static. However, in the case of HD, we face an additional complication: if the HD column density is sufficiently high for HD self-shielding to be significant, then the H_2 column density will be very much larger (since even in significantly fractionated regions, one typically has an HD: H_2 ratio of no more than about 10^{-3}). Consequently, the line widths of the H_2 Lyman-Werner lines are not negligible, and some degree of overlap between these lines and the HD absorption lines will occur. Additionally, if the H_2 :H ratio is small, as will often be the case in the systems of interest, then a significant HD column density implies a large neutral hydrogen column density, which means that absorption of radiation in the Lyman series lines of atomic hydrogen must also be taken into account.

These effects are difficult to include accurately in a simple treatment of HD self-shielding and before attempting to do so it is reasonable to ask whether an accurate treatment of HD self-shielding is really required. We argue that in many cases of interest it is not. Comparison of the rate at which HD is photodissociated in optically thin gas with the rate at which it is destroyed by reaction 21 demonstrates that the latter dominates whenever $n_{\text{H}^+} \gtrsim 10^{-3} J_{21}(\bar{\nu})$, where $J_{21}(\bar{\nu})$ is the strength of the radiation field at $h\bar{\nu} = 12.87$ eV in units of $10^{-21} \text{ ergs s}^{-1} \text{ cm}^{-2} \text{ Hz}^{-1} \text{ sr}^{-1}$. Photodissociation therefore dominates only when the UV field is strong or the proton number density is small. However, in either case, it is difficult to see how the large column densities of HD and H_2 required for effective shielding could be built up or maintained. Therefore, we suspect that for most applications, treating the HD in the optically thin limit is probably sufficient, as in the conditions where this approximation breaks down, photodissociation is unlikely to be important.

3. Thermal processes

3.1. Fine structure cooling

As we do not include molecular coolants such as CO or H_2O in our chemical model of metal-enriched gas, for the reasons outlined in §2.1, the main contribution that the metals make to the cooling of the gas is through fine structure line emission from neutral C, O and Si atoms and C^+ and Si^+ ions. To model this emission, we assume that the populations of all the electronically excited levels of these atoms and ions are negligible, an approximation which should be highly accurate at the gas densities considered in this study. This assumption allows us to model C^+ and Si^+ as two-level systems and C, O and Si as three-level systems, allowing us to compute their effects in a straightforward fashion. For a two-level ion, if we denote the ground state as level 0 and the excited state as level 1, then the power radiated

per unit volume can be written as

$$\Lambda = (A_{10} + B_{10}I_{10})E_{10}n_1, \quad (52)$$

where n_1 is the number density of ions in level 1, A_{10} is the Einstein coefficient for spontaneous emission for the transition from level 1 to level 0, B_{10} is the corresponding coefficient for stimulated emission, E_{10} is the energy of the transition, and I_{10} is the mean specific intensity at the frequency of the transition. If $I_{10} \neq 0$, then the ions will also absorb energy from the radiation field, at a rate

$$\Gamma = B_{01}I_{10}E_{10}n_0, \quad (53)$$

where n_0 is the number density of ions in level 0 and B_{01} is the Einstein coefficient for absorption from level 0 to level 1, which is related to B_{10} by $B_{01} = (g_1/g_0)B_{10}$, where g_0 and g_1 are the statistical weights of levels 0 and 1 respectively. The net loss of energy per unit time per unit volume is therefore

$$\begin{aligned} \Lambda' &= \Lambda - \Gamma \\ &= E_{10}\{A_{10}n_1 + B_{10}I_{10}[n_1 - (g_1/g_0)n_0]\}, \end{aligned} \quad (54)$$

and it will be seen that if

$$n_0 > \frac{A_{10} + B_{10}I_{10}}{(g_1/g_0)B_{10}I_{10}}n_1, \quad (55)$$

then the ions will absorb more energy than they emit, and so the gas will actually gain energy.

To compute Λ' , we need to know several pieces of atomic data – the values of A_{10} , E_{10} , g_0 and g_1 , which are summarized for C^+ and Si^+ in Table 5 – together with the values of I_{01} , n_0 and n_1 . To compute n_0 and n_1 , we assume that the levels are in statistical equilibrium, in which case:

$$(B_{01}I_{01} + C_{01})n_0 = (A_{10} + B_{10}I_{10} + C_{10})n_1, \quad (56)$$

where C_{01} and C_{10} are the total rates of collisional excitation and de-excitation respectively. These are related by

$$C_{01} = C_{10} \frac{g_1}{g_0} \exp\left(-\frac{E_{10}}{kT}\right), \quad (57)$$

and so once one is known, the other can be computed easily. In Table 6, we list collisional de-excitation rates for collisions between C^+ or Si^+ and various possible collision partners such as H, H_2 or e^- . Given the number densities of these species, C_{10} can be easily computed, since

$$C_{10} = \sum_k q_{10,k}n_k, \quad (58)$$

where $q_{10,k}$ is the collisional de-excitation rate for a collision with chemical species k with number density n_k . For C^+ , we include the effects of collisions with electrons, atomic hydrogen and molecular hydrogen (in both ortho and para forms). The collision rate with H^+ is negligible at the temperatures of interest due to the strong Coloumb repulsion, and the abundances of the other chemical species included in our model are too small for them to be important collision partners. For Si^+ , we include only the effects of collisions with H and e^- , as rates for collisions with H_2 are not available. However, provided that the H_2 abundance is small compared to the atomic hydrogen abundance, this is unlikely to be a major source of error.

Finally, to compute I_{10} , we assume that the only significant radiation field present at the infra-red and sub-millimeter wavelengths of the fine structure transitions is the cosmic microwave background. In that case, I_{10} is simply given by the value of the Planck function at the frequency of the transition for a radiation field with temperature $T = T_{\text{CMB}} = 2.726(1+z)$ K.

For the three-level atoms (C, O and Si), we use a very similar approach. In this case, the power radiated per unit volume is

$$\Lambda = (A_{10} + B_{10}I_{10})E_{10}n_1 + (A_{20} + B_{20}I_{20})E_{20}n_2 + (A_{21} + B_{21}I_{21})E_{21}n_2, \quad (59)$$

and the power absorbed per unit volume is

$$\Gamma = B_{01}I_{10}E_{10}n_0 + B_{02}I_{20}E_{20}n_0 + B_{12}I_{21}E_{21}n_1, \quad (60)$$

where 0, 1 and 2 denote the ground state and the two excited states respectively. The level populations n_0 , n_1 and n_2 are found by solving

$$(B_{01}I_{01} + C_{01} + B_{02}I_{02} + C_{02})n_0 = (A_{10} + B_{10}I_{10} + C_{10})n_1 + (A_{20} + B_{20}I_{20} + C_{20})n_2, \quad (61)$$

$$(B_{10}I_{10} + C_{10} + B_{12}I_{12} + C_{12})n_1 = (B_{01}I_{01} + C_{01})n_0 + (A_{21} + B_{21}I_{21} + C_{21})n_2, \quad (62)$$

with all symbols having their obvious meanings. To compute the total collisional excitation and de-excitation rates for carbon and oxygen we include the effects of collisions with ortho and para- H_2 , atomic hydrogen, protons and electrons. For silicon, we include only the effects of collisions with H and H^+ , as rates for collisions with H_2 or electrons do not appear to be available. The rates used are summarized in Table 6.

3.2. Other coolants

Apart from fine structure emission, we also include in our thermal model several other processes that can lead to the cooling of the gas. These are summarized in Table 7, along

with a reference to the source (or sources) from which the associated cooling rate has been taken. In most cases, the rate itself is also listed.

In hot, ionized gas, cooling is dominated by electron impact excitation of atomic hydrogen (Lyman- α cooling), atomic helium and He^+ . Excitation of atomic helium occurs from both the 1^1S ground state and the 2^3S metastable state. In common with previous authors, we assume that the population of the 2^3S state is set by the balance between radiative recombination to triplet states and radiative decay to the ground state. One consequence of this assumption is that the number density of He atoms in the 2^3S state, $n_{\text{He}(2^3\text{S})}$, is proportional to the product of the number densities of free electrons and of He^+ , i.e. $n_{\text{He}(2^3\text{S})} \propto n_e n_{\text{He}^+}$, which means that the cooling rate from metastable helium scales as $n_{\text{He}(2^3\text{S})} n_e \propto n_e^2 n_{\text{He}^+}$. To model cooling from H, the He metastable state, and He^+ , we use rates from Cen (1992), which themselves were based on earlier work by Black (1981). To model cooling from the He ground state, we use our own fit to the data of Bray et al. (2000).

A number of other processes are of importance in ionized gas. We include cooling due to collisional ionization of atomic hydrogen and atomic helium, the gas phase recombination of H^+ and He^+ , ionic recombination on dust grains, Compton scattering of CMB photons by free electrons (Compton cooling), and thermal bremsstrahlung. The rates adopted for all of these processes are summarized in Table 7. As the chemical and thermal model presented here is not designed to be used for the study of very hot gas, we do not include processes involving He^{++} (although rates for these processes can be found in Cen 1992).

In neutral gas, all of the aforementioned processes become ineffective. In cool, neutral gas, most of the cooling comes from H_2 or from the fine structure lines of carbon, oxygen and silicon, which have already been discussed above. Cooling from H_2 is treated in our model through use of the cooling function of Le Bourlot et al. (1999), which we have extended to temperatures below 100 K by assuming that only the $J = 2 \rightarrow 0$ and $J = 3 \rightarrow 1$ transitions contribute significantly to the cooling rate. Le Bourlot et al. (1999) tabulate the H_2 cooling rate as a function of temperature, density, H: H_2 ratio and ortho:para ratio. For simplicity, in our implementation we do not track the evolution of the H_2 ortho:para ratio, instead keeping it fixed at 3:1, but we note that variations in this ratio are unlikely to significantly affect the H_2 cooling rate at temperatures at which it contributes significantly to the total cooling rate (see, for instance, figure 5 in Le Bourlot et al. 1999). A comparison of the Le Bourlot et al. H_2 cooling rate with various other rates that have been used in the literature is given in paper II (Figure 1).

At low temperatures ($T \lesssim 200$ K), HD cooling becomes increasingly important and can dominate the total cooling rate if sufficient fractionation occurs (Galli & Palla 1998). To model HD cooling, we use the recent cooling function of Lipovka, Núñez-López, & Avila-Reese

(2005). They provide a complicated fit as a value of temperature and density that is valid over a wide range of both. For further details, the interested reader should consult their paper.

We include two final processes that can become important in some circumstances. Cooling due to H_2 collisional dissociation is modelled under the assumption that each dissociation removes ~ 4.48 eV of thermal energy from the gas. It is an effective source of cooling only at temperatures above a few thousand Kelvin. In practice, the H_2 abundance in zero metallicity or low metallicity gas is frequently too small for this process to be important.

We also include the effects of energy transfer from the gas to the dust grains (if present), using a rate from Hollenbach & McKee (1989). At solar metallicity, this becomes important at a density $n \sim 10^4 \text{ cm}^{-3}$, but at lower metallicities, it does not dominate until significantly larger densities are reached (see e.g. Omukai et al. 2005).

3.3. Heating

We include in our model the effects of several processes that can heat the gas. Most of these processes operate only if a radiation background is present. The first of these is photoelectric emission from dust grains. This operates as follows: photons that interact with dust grains can cause the ejection of energetic electrons from the grain if the photon energy exceeds the work function of the grain. As the energy carried by the electrons is quickly thermalized, this leads to the heating of the gas. This process is of great importance in the local ISM and has been examined in detail by a number of authors (e.g. Bakes & Tielens 1994; Wolfire *et al.* 1995; Weingartner & Draine 2001b; Rae et al. 2004).

To accurately compute the effects of photoelectric emission, we need to know the grain size distribution and the composition of the grains. However, as discussed previously, large uncertainties exist concerning the properties of grains in low metallicity protogalactic gas. We therefore make the same assumption here as we did in our treatment of grain surface chemistry, i.e. that the dust has the same properties as Milky Way dust, but has an abundance that is reduced by a factor (Z/Z_\odot) . This assumption allows us to use the following expression for the photoelectric heating rate, taken from Wolfire *et al.* (1995):

$$\Gamma_{\text{pe}} = 1.3 \times 10^{-24} \epsilon G \left(\frac{Z}{Z_\odot} \right) n \text{ erg s}^{-1} \text{ cm}^{-3}, \quad (63)$$

where $G \simeq 0.01 J_{21}$ is a measure of the radiation energy density between 6 eV and 13.6 eV relative to the Habing (1968) field, and where ϵ is the photoelectric heating efficiency, given

by

$$\epsilon = \frac{4.9 \times 10^{-2}}{1.0 + 4.0 \times 10^{-3} \tilde{\psi}^{0.73}} + \frac{3.7 \times 10^{-2} T_4^{0.7}}{1.0 + 2.0 \times 10^{-4} \tilde{\psi}}, \quad (64)$$

where $T_4 = T/10^4$ K. The parameter $\tilde{\psi}$ that controls the photoelectric heating efficiency is given by $\tilde{\psi} = G\sqrt{T}/0.5n_e$ (Wolfire *et al.* 2003); note that this differs by a factor of 2 from the parameter ψ introduced in §2.3. For small $\tilde{\psi}$, most grains are negatively charged and $\epsilon \simeq 4.9 \times 10^{-2} + 3.7 \times 10^{-2} T_4^{0.7}$. On the other hand, for large $\tilde{\psi}$, most grains are positively charged, and ϵ is small, as it is difficult for photons with energies $E < 13.6$ eV to dislodge further electrons from the grains.

A second source of radiative heating is the photodissociation of H_2 . Our treatment of photodissociation heating follows Black & Dalgarno (1977): we assume that each photodissociation deposits 0.4 eV of thermal energy into the gas. As well as photodissociating some of the H_2 , an ultraviolet background will also produce vibrationally excited H_2 via radiative pumping of the excited levels. In dense gas, this pumping leads to heating as most of the excited molecules undergo collisional de-excitation. We include the effects of radiative pumping by adopting a pumping rate that is 8.5 times larger than the photodissociation rate (Draine & Bertoldi 1996), and assuming that each excitation transfers an average of $2(1 + n_{\text{cr}}/n)^{-1}$ eV to the gas (Burton *et al.* 1990), where n_{cr} is the critical density at which collisional de-excitation of vibrationally excited H_2 occurs at the same rate as radiative de-excitation. Our value for n_{cr} is a weighted harmonic mean of the value for H_2 -H collisions given by Lepp & Shull (1983), reduced by a factor of ten as advised by Martin, Schwarz & Mandy (1996), and the value for H_2 - H_2 collisions given by Shapiro & Kang (1987).

Heating due to the photoionization of H or He has already been discussed in §2.4 and we do not discuss it further here. As is also discussed in that section, we do not include heating due to the photodetachment of H^- , photodissociation of H_2^+ or photoionization of C, O, Si or Si^+ , as the contribution from these processes is not significant.

We also include the effects of heating due to H_2 formation. The formation of an H_2 molecule via reaction 2 releases 3.53 eV of energy, while formation via reaction 4 releases 1.83 eV, and formation on a grain surface (reaction 60) releases 4.48 eV. We assume that essentially all of this energy goes into rotational and vibrational excitation of the resulting H_2 molecule, and hence is radiated away at low gas densities and is converted by collisional de-excitation into heat at high gas densities.

Finally, we include heating due to the ionization of the gas by cosmic rays. Following Goldsmith & Langer (1978), we assume that every ionization deposits 20 eV of heat in the gas, and so derive a heating rate that scales with the total cosmic ray ionization rate of

the gas (i.e. the sum of the ionization rates for the various individual chemical species, weighted by the fractional abundances of those species). Since considerable uncertainty exists concerning the value of the cosmic ray ionization rate in the local interstellar medium (see the discussion in McCall et al. 2003), let alone concerning the appropriate rate to use in high-redshift protogalaxies, a more detailed treatment does not appear to be warranted at this time.

4. Applications

The chemical network and thermal model described in the preceding sections have a number of potential applications. One of the more obvious applications is the study of the cooling and gravitational collapse of gas in low metallicity protogalaxies. As previously noted, the density range for which our model is valid corresponds to a wide range of cosmological overdensities. It can therefore be used to study the thermal and chemical evolution of the majority of the gas within a given protogalaxy. For example, suppose we model the gas distribution within a $z = 20$ halo as a singular isothermal sphere with mean number density within the virial radius $\bar{n} = 0.4 \text{ cm}^{-3}$ (a reasonable zeroth-order approximation for a protogalactic halo with a mean overdensity $\delta = 200$; see e.g. Abel et al. 2002). In this case, only $\sim 4\%$ of the gas within the halo has a density $n > 100 \text{ cm}^{-3}$ at which our model may break down. Therefore, although our model is of limited usefulness for studying gravitational fragmentation and star formation within this dense central region, it does allow one to study many other important problems, such as how the minimum protogalactic mass at which cooling becomes effective is affected by the presence of metals, or how the gas responds to the presence of an ultraviolet background. We use a version of this model to address some of these questions in paper II for the case of small protogalactic halos within initially ionized regions.

A second possible application is the study of the evolution of the ISM in high redshift, metal-poor dwarf galaxies. In this case, much of the gas involved is often gravitationally stable, and so the characteristic timescales are longer than the gravitational free-fall time. This limits the applicability of the model to lower densities than in the case of gravitationally collapsing protogalaxies. However, even if we adopt a relatively long characteristic timescale $t_{\text{char}} = 100 \text{ Myr}$, corresponding to the sound crossing time of a 1 kpc disk at a sound speed of 10 km s^{-1} , the model remains valid for densities up to $n \sim 5 \text{ cm}^{-3}$ even in the least auspicious case ($Z = 0.1 Z_{\odot}$ gas, with no significant UV radiation field present). Our model is therefore well-suited for use in the study of the evolution of the warm neutral component of the ISM in such galaxies and will in some cases also be useful in the study of the cold

neutral component. However, the reader is reminded that our model does not treat hot ($T \gg 10^4$ K), highly-ionized gas, and cannot be used to study the effects of stellar feedback (H II regions, supernovae, etc.) unless coupled with some existing model capable of treating this hot gas (see e.g. Sutherland & Dopita 1993).

As well as studying the chemical evolution of gas *within* dwarf galaxies and protogalaxies, we can also use it to study the chemical evolution of gas *between* galaxies, i.e. the intergalactic medium (IGM). One important reason to do so is the fact that several different observational techniques have been suggested that may allow one to probe the thermal and chemical state of this gas. Oh (2002) has suggested that if large regions of the IGM remain neutral after the turn-on of the first observable ionizing sources, then atomic oxygen in the IGM may be detectable through its UV absorption, as it will produce an O I forest analogous to the $z < 6$ H I Lyman- α forest. Furlanetto & Loeb (2003) also argue that a substantial fraction of the metals in high-redshift Galactic winds are likely to be in low-ionization states and may be observable in absorption. Metals in the high redshift IGM may also leave detectable imprints in the fluctuation spectrum of the cosmic microwave background (Basu et al 2004; Hernández-Monteagudo et al. 2006). Finally, Hernández-Monteagudo et al. (2007) have recently suggested that fine structure emission from atomic oxygen may also produce a detectable spectral distortion of the CMB if the excited fine-structure levels can be populated by radiative pumping via the O I Balmer- α transition. Accurate modelling of many of these effects requires accurate modelling of the temperature and chemical make-up of the intergalactic gas, and hence a model such as that presented here.

We thank R. Klessen and M.-M. Mac Low for useful discussions, and the anonymous referee for valuable feedback on earlier drafts of this paper. S.C.O.G. acknowledges support from NSF grant AST03-07793 during the early phases of this work. A.K.J. acknowledges support from the Emmy Noether Program of the Deutsche Forschungsgemeinschaft (grant no. KL1358/1).

REFERENCES

- Abel, T., Anninos, P., Zhang, Y., & Norman, M. L. 1997, *New Astron.*, 2, 181
- Abel, T., Bryan, G. L., & Norman, M. L. 2002, *Science*, 295, 93
- Abgrall, H., Roueff, E., Launay, F., Roncin, J.-Y., & Subtil, J.-L. 1993a, *A&AS*, 101, 273
- Abgrall, H., Roueff, E., Launay, F., Roncin, J.-Y., & Subtil, J.-L. 1993b, *A&AS*, 101, 323

- Abgrall, H., Roueff, E., & Drira, I. 2000, A&AS, 141, 297
- Abgrall, H., & Roueff, E. 2006, A&A, 445, 361
- Ahn, K., & Shapiro, P. R. 2007, MNRAS, 375, 881
- Aldrovandi, S. M. V. & Pequignot, D. 1973, A&A, 25, 137
- Asplund, M., Grevesse, N., & Sauval, J. 2006, Nucl. Phys. A, 777, 1
- Bakes, E. L. O., & Tielens, A. G. G. M. 1994, ApJ, 427, 822
- Barlow, S. G. 1984, PhD thesis, Univ. Colorado
- Basu, K., Hernández-Monteagudo, C., & Sunyaev, R. A. 2004, A&A, 416, 447
- Bell, K. L., Berrington K. A., & Thomas, M. R. J. 1998, MNRAS, 293, L83
- Black, J. H. & Dalgarno, A. 1977, ApJS, 34, 405
- Black, J. H. 1981, MNRAS, 197, 553
- Black, J. H. 1991, in T. W. Hartquist (ed.), *Molecular Astrophysics*, Cambridge University Press, Cambridge, U.K., p. 473
- Bray, I., Burgess, A., Fursa, D. V., & Tully, J. A. 2000, A&AS, 148, 481
- Bromm, V., Ferrara, A., Coppi, P. S., & Larson, R. B. 2001, MNRAS, 328, 969
- Bromm, V. & Loeb, A. 2003, Nature, 425, 812
- Burton, M. G., Hollenbach, D. J., & Tielens, A. G. G. M. 1990, ApJ, 365, 620
- Cazaux, S., & Spaans, M. 2004, ApJ, 611, 40
- Cazaux, S., & Tielens, A. G. G. M. 2004, ApJ, 604, 222
- Cen, R. 1992, ApJS, 78, 341
- Dalgarno, A., & Lepp, S. 1987, in *Astrochemistry*, ed. M. S. Vardya & S. P. Tarafdar (Dordrecht: Reidel), 109
- Dalgarno, A., Yan, M., Liu, W. 1999, ApJS, 125, 237
- de Jong, T. 1972, A&A, 20, 263
- Dove, J. E., Rusk, A. C. M., Cribb, P. H., & Martin, P. G. 1987, ApJ, 318, 379

- Draine, B. T., & Bertoldi, F. 1996, *ApJ*, 468, 269
- Dufton, P. L. & Kingston, A. E. 1991, *MNRAS*, 248, 827
- Dunn, G. H. 1968, *Phys. Rev.*, 172, 1
- Ferland, G. J., Peterson, B. M., Horne, K., Welsh, W. F., & Nahar, S. N. 1992, *ApJ*, 387, 95
- Field, G. B., Somerville, W. B., & Dressler, K. 1966, *ARA&A*, 4, 207
- Flower, D. R. & Launay, J. M. 1977, *J. Phys. B*, 10, 3673
- Flower, D. R., Le Bourlot, J., Pineau des Forêts, G., & Roueff, E. 2000, *MNRAS*, 314, 753
- Frebel, A., Johnson, J. L., & Bromm, V. 2007, *astro-ph/0701395*
- Furlanetto, S. R., & Loeb, A. 2003, *ApJ*, 588, 18
- Galli, D., & Palla, F. 1998, *A&A*, 335, 403
- Gerlich, D. 1982, in ‘Symposium on Atomic and Surface Physics’, eds. Lindinger, W., Howorka, F., Märk, T. D., (Dordrecht: Kluwer), p. 304
- Glover, S. C. O. 2001, PhD thesis, University of Edinburgh
- Glover, S. C. O. 2003, *ApJ*, 584, 331
- Glover, S. C. O. 2007, *MNRAS*, accepted; *astro-ph/0703716*
- Glover, S. C. O. & Brand, P. W. J. L. 2003, *MNRAS*, 340, 210
- Glover, S. C. O., & Mac Low, M.-M. 2007a, *ApJS*, 169, 239
- Glover, S. C. O., & Mac Low, M.-M. 2007b, *ApJ*, 659, 1317
- Glover, S. C. O. & Savin, D. W. 2006, *Phil. Trans. Roy. Soc. Lon. A*, 364, 3107
- Glover, S. C. O. & Savin, D. W. 2007, in preparation
- Glover, S. C. O., Savin, D. W., & Jappsen, A.-K. 2006, *ApJ*, 640, 553
- Goldsmith, P., & Langer, W. D. 1978, *ApJ*, 222, 881
- Habing, H. J. 1968, *Bull. Astron. Inst. Netherlands*, 19, 421
- Hasegawa, T. I., Herbst, E., & Leung, C. M. 1992, *ApJS*, 82, 167

- Heger, A., & Woosley, S. E. 2002, *ApJ*, 567, 532
- Hernández-Monteagudo, C., Rubino-Martin, J. A. & Sunyaev, R. A. 2006, *astro-ph/0611497*
- Hernández-Monteagudo, C., Haiman, Z., Jimenez, R., & Verde, L. 2007, 660, L85
- Hirashita, H., & Ferrara, A. 2002, *MNRAS*, 337, 921
- Hollenbach, D., & McKee, C. F. 1979, *ApJS*, 41, 555
- Hollenbach, D., & McKee, C. F. 1989, *ApJ*, 342, 306
- Hosokawa, T., & Inutsuka, S. 2006, *ApJ*, 646, 240
- Hummer, D. G., & Storey, P.J. 1998, *MNRAS*, 297, 1073
- Janev, R. K., Langer, W. D., Evans, K., & Post, D. E. 1987, *Elementary Processes in Hydrogen-Helium Plasmas*, Springer
- Jappsen, A.-K., Glover, S. C. O., Klessen, R. S., & Mac Low, M.-M. 2007, *ApJ*, 660, 1332. (Paper II)
- Johnson, C. T., Burke, P. G., & Kingston, A. E. 1987, *J. Phys. B*, 20, 2553
- Julienne, P. S., Krauss, M., & Donn, B. 1971, *ApJ*, 170, 65
- Karpas, Z., Anicich, V., & Huntress, W. T. 1979, *J. Chem. Phys.*, 70, 2877
- Keenan, F. P., Lennon, D. J., Johnson, C. T. & Kingston, A. E. 1986, *MNRAS*, 220, 571
- Kimura, M., Lane, N. F., Dalgarno, A., & Dixon, R. G. 1993, *ApJ*, 405, 801
- Kimura, M., Dalgarno, A., Chanturanupong, L., Li, Y., Hirsch, G., & Buenker, R. J. 1993, *ApJ*, 417, 812
- Kingdon, J. B. & Ferland, G. J. 1996, *ApJS*, 106, 205
- Langer, W. D. 1978, *ApJ*, 225, 860
- Launay, J. M., Le Dourneuf, M., & Zeippen, C. J. 1991, *A&A*, 252, 842
- Le Bourlot, J., Pineau des Forêts, G., & Flower, D. R. 1999, *MNRAS*, 305, 802
- Lepp, S., & Shull, J. M. 1983, *ApJ*, 270, 578
- Lepp, S. H., Stancil, P. C., & Dalgarno, A. 2002, *J. Phys. B*, 35, 57

- Le Teuff, Y. H., Millar, T. J., & Markwick, A. J. 2000, *A&AS*, 146, 157
- Lipovka, A., Núñez-López, R., & Avila-Reese, V. 2005, *MNRAS*, 361, 850
- Lotz, W. 1967, *ApJS*, 14, 207
- Mac Low, M.-M., & Shull, J. M. 1986, *ApJ*, 302, 585
- Machacek, M. E., Bryan, G. L., & Abel, T. 2001, *ApJ*, 548, 509
- Machacek, M. E., Bryan, G. L., & Abel, T. 2003, *MNRAS*, 338, 273
- Martin, P. G., Schwarz, D. H., & Mandy, M. E. 1996, *ApJ*, 461, 265
- Martin, P. G., Keogh W. J., & Mandy, M. E. 1998, *ApJ*, 499, 793
- Mathis, J. S., Rumpl, W., & Nordsieck, K. H. 1977, *ApJ*, 217, 425
- Matsuda, T., Satō, H., & Takeda, H. 1969, *Prog. Th. Phys.*, 42, 219
- Mazzotta, P., Mazzitelli, G., Colafrancesco, S., & Vittorio, N. 1998, *A&AS*, 133, 403
- McCall, B. J., et al. 2003, *Nature*, 422, 500
- Mielke, S. L., Lynch, G. C., Truhlar, D. G., & Schwenke, D. W. 1994, *J. Phys. Chem.*, 98, 8000
- Mizusawa, H., Omukai, K., & Nishi, R. 2005, *PASJ*, 57, 951
- Moseley, J., Aberth, W., & Peterson, J. R. 1970, *Phys. Rev. Lett.*, 24, 435
- Nahar, S. N. 1995, *ApJS*, 101, 423
- Nahar, S. N. 1996, *ApJS*, 106, 213
- Nahar, S. N. 1999, *ApJS*, 120, 131
- Nahar, S. N. 2000, *ApJS*, 126, 537
- Nahar, S. N. & Pradhan, A. K. 1997, *ApJS*, 111, 339
- Neufeld, D. A., & Kaufman, M. J. 1993, *ApJ*, 418, 263
- Neufeld, D. A., Lepp., S., & Melnick, G. J. 1995, *ApJS*, 100, 132
- Nozawa, T., Kozasa, T., Umeda, H., Maeda, K., & Nomoto, K. 2003, *ApJ*, 598, 785

- Oh, S. P. 2002, MNRAS, 336, 1021
- Omukai, K., Tsuribe, T., Schneider, R., & Ferrara, A. 2005, ApJ, 626, 627
- O’Neil, S. V., & Reinhardt, W. P. 1978, J. Chem. Phys., 69, 2126
- Osterbrock, D. E. 1989, Astrophysics of Gaseous Nebulae and Active Galactic Nuclei, University Science Books.
- Peebles, P. J. E. & Dicke, R. H. 1968, ApJ, 154, 891
- Pequignot, D. 1990, A&A, 231, 499
- Pequignot, D. 1996, A&A, 313, 1026
- Poulaert, G., Brouillard, F., Claeys, W., McGowan, J. W., & Van Wassenhove, G. 1978, J. Phys. B, 11, L671
- Rae, J. G. L., Hartquist, T. W., Lepp, S. H., O’Neill, P. T., & Williams, D. A. 2004, A&A, 413, 1
- Ramaker, D. E., & Peek, J. M. 1976, Phys. Rev. A, 13, 58
- Roueff, E. 1990, A&A, 234, 567
- Roueff, E. & Le Bourlot, J. 1990, A&A, 236, 515
- Santoro, F. & Shull, J. M. 2006, ApJ, 643, 26
- Saslaw, W. C. & Zipoy, D. 1967, Nature, 216, 976
- Savin, D. W. 2002, ApJ, 566, 599
- Savin, D. W., Krstic, P. S., Haiman, Z., & Stancil, P. C. 2004, ApJ, 606, L167; erratum ApJ, 607, L147
- Schneider, I. F., Dulieu, O., Giusti-Suzor, A., & Roueff, E. 1994, ApJ, 424, 983; erratum ApJ, 486, 580
- Schneider, R., Ferrara, A., Natarajan, P. & Omukai, K. 2002, ApJ, 571, 30
- Schneider, R., Ferrara, A., & Salvaterra, R. 2004, MNRAS, 351, 1379
- Schneider, R., Omukai, K., Inoue, A., & Ferrara, A., 2006, MNRAS, 369, 1437

- Schroder, K., Staemmler, V., Smith, M. D., Flower, D. R., & Jaquet, R. 1991, *J. Phys. B*, 24, 2487
- Sembach, K. R., Howk, J. C., Ryans, R. S. I., & Keenan, F. P. 2000, *ApJ*, 528, 310
- Shapiro, P. R., & Kang, H. 1987, *ApJ*, 318, 32
- Shavitt, I. 1959, *J. Chem. Phys.*, 31, 1359
- Shull, J. M. 1978, *ApJ*, 219, 877
- Shull, J. M., & van Steenberg, M. E. 1985, *ApJ*, 298, 268
- Silva, A. I., & Viegas, S. M. 2002, *MNRAS*, 329, 135
- Smith, W. H., & Zweibel, E. G. 1976, *ApJ*, 207, 758
- Stancil, P. C., Lepp, S., & Dalgarno, A. 1998, *ApJ*, 509, 1
- Stancil, P. C., Havener, C. C., Krstic, P. S., Schultz, D. R., Kimura, M., Gu, J.-P., Hirsch, G., Buenker, R. J., & Zygelman, B. 1998, *ApJ*, 502, 1006
- Stancil, P. C., Schultz, D. R., Kimura, M., Gu, J.-P., Hirsch, G., & Buenker, R. J. 1999, *A&AS*, 140, 225
- Stecher, T. P., & Williams, D. A. 1967, *ApJ*, 149, L29
- Stibbe, D. T., & Tennyson, J. 1999, *ApJ*, 513, L147
- Sutherland, R. S., & Dopita, M. A. 1993, *ApJS*, 88, 253
- Tegmark, M., Silk, J., Rees, M. J., Blanchard, A., Abel, T., & Palla, F. 1997, *ApJ*, 474, 1
- Todini, P., & Ferrara, A. 2001, *MNRAS*, 325, 726
- Tumlinson, J., Venkatesan, A., & Shull, J. M. 2004, *ApJ*, 612, 602
- Venkatesan, A., Nath, B. B., & Shull, J. M. 2006, *ApJ*, 640, 31
- Verner, D. A., Ferland, G. J., Korista, K. T. & Yakovlev, D. G. 1996, *ApJ*, 465, 487
- Voronov, G. S. 1997, *ADNDT*, 65, 1
- Wagner, A. F., & Graff, M. M. 1987, *ApJ*, 317, 423
- Wakker, B. P. 2006, *ApJS*, 163, 282

- Weingartner, J. C. & Draine, B. T. 2001a, *ApJ*, 563, 842
- Weingartner, J. C. & Draine, B. T. 2001b, *ApJS*, 134, 263
- Wilms, J., Allen, A., & McCray, R. 2002, *ApJ*, 542, 914
- Wilson, N. J. & Bell, K. L. 2002, *MNRAS*, 337, 1027
- Wishart, A. W. 1979, *MNRAS*, 187, 59P
- Wolfire, M. G., Hollenbach, D., McKee, C. F., Tielens, A. G. G. M., & Bakes, E. L. O. 1995, *ApJ*, 443, 152
- Wolfire, M. G., McKee, C. F., Hollenbach, D., & Tielens, A. G. G. M. 2003, *ApJ*, 587, 278
- Yan, M., Sadeghpour, H. R., & Dalgarno, A. 1998, *ApJ*, 496, 1044
- Yoshida, N., Abel, T., Hernquist, L., & Sugiyama, N. 2003, *ApJ*, 592, 645
- Zhao, L. B., Stancil, P. C., Gu, J. P., Liebermann, H.-P., Li, Y., Funke, P., Buenker, R. J., Zygelman, B., Kimura, M., & Dalgarno, A. 2004, *ApJ*, 615, 1063
- Zygelman, B., Dalgarno, A., Kimura, M., & Lane, N. F. 1989, *Phys. Rev. A*, 40, 2340

Table 1. List of the collisional gas-phase reactions in our chemical model.

No.	Reaction	Rate coefficient ($\text{cm}^3 \text{s}^{-1}$)	Ref.
1	$\text{H} + \text{e}^- \rightarrow \text{H}^- + \gamma$	$k_1 = \text{dex}[-17.845 + 0.762 \log T + 0.1523(\log T)^2 - 0.03274(\log T)^3]$ $T \leq 6000 \text{ K}$ $= \text{dex}[-16.420 + 0.1998(\log T)^2 - 5.447 \times 10^{-3}(\log T)^4 + 4.0415 \times 10^{-5}(\log T)^6]$ $T > 6000 \text{ K}$	1
2	$\text{H}^- + \text{H} \rightarrow \text{H}_2 + \text{e}^-$	$k_2 = 1.5 \times 10^{-9}$ $T \leq 300 \text{ K}$ $= 4.0 \times 10^{-9} T^{-0.17}$ $T > 300 \text{ K}$	2
3	$\text{H} + \text{H}^+ \rightarrow \text{H}_2^+ + \gamma$	$k_3 = \text{dex}[-19.38 - 1.523 \log T + 1.118(\log T)^2 - 0.1269(\log T)^3]$	3
4	$\text{H} + \text{H}_2^+ \rightarrow \text{H}_2 + \text{H}^+$	$k_4 = 6.4 \times 10^{-10}$	4
5	$\text{H}^- + \text{H}^+ \rightarrow \text{H} + \text{H}$	$k_5 = 5.7 \times 10^{-6} T^{-0.5} + 6.3 \times 10^{-8} - 9.2 \times 10^{-11} T^{0.5} + 4.4 \times 10^{-13} T$	5
6	$\text{H}_2^+ + \text{e}^- \rightarrow \text{H} + \text{H}$	$k_6 = 1.0 \times 10^{-8}$ $T \leq 617 \text{ K}$ $= 1.32 \times 10^{-6} T^{-0.76}$ $T > 617 \text{ K}$	6
7	$\text{H}_2 + \text{H}^+ \rightarrow \text{H}_2^+ + \text{H}$	$k_7 = [-3.3232183 \times 10^{-7} + 3.3735382 \times 10^{-7} \log T - 1.4491368 \times 10^{-7}(\log T)^2 + 3.4172805 \times 10^{-8}(\log T)^3 - 4.7813720 \times 10^{-9}(\log T)^4 + 3.9731542 \times 10^{-10}(\log T)^5 - 1.8171411 \times 10^{-11}(\log T)^6]$	7

Table 1—Continued

No.	Reaction	Rate coefficient (cm ³ s ⁻¹)	Ref.
		$+ 3.5311932 \times 10^{-13}(\log T)^7]$ $\times \exp\left(\frac{-21237.15}{T}\right)$	
8	$\text{H}_2 + \text{e}^- \rightarrow \text{H} + \text{H} + \text{e}^-$	$k_8 = 3.73 \times 10^{-9} T^{0.1121} \exp\left(\frac{-99430}{T}\right)$	8
9	$\text{H}_2 + \text{H} \rightarrow \text{H} + \text{H} + \text{H}$	$k_9 = 6.67 \times 10^{-12} T^{1/2} \exp\left[-(1 + \frac{63590}{T})\right]$	9
10	$\text{H}_2 + \text{H}_2 \rightarrow \text{H}_2 + \text{H} + \text{H}$	$k_{10} = \frac{5.996 \times 10^{-30} T^{4.1881}}{(1.0 + 6.761 \times 10^{-6} T)^{5.6881}} \exp\left(-\frac{54657.4}{T}\right)$	10
11	$\text{H} + \text{e}^- \rightarrow \text{H}^+ + \text{e}^- + \text{e}^-$	$k_{11} = \exp[-3.271396786 \times 10^1$ $+ 1.35365560 \times 10^1 \ln T_e$ $- 5.73932875 \times 10^0 (\ln T_e)^2$ $+ 1.56315498 \times 10^0 (\ln T_e)^3$ $- 2.87705600 \times 10^{-1} (\ln T_e)^4$ $+ 3.48255977 \times 10^{-2} (\ln T_e)^5$ $- 2.63197617 \times 10^{-3} (\ln T_e)^6$ $+ 1.11954395 \times 10^{-4} (\ln T_e)^7$ $- 2.03914985 \times 10^{-6} (\ln T_e)^8]$	11
12	$\text{D} + \text{e}^- \rightarrow \text{D}^+ + \text{e}^- + \text{e}^-$	$k_{12} = k_{11}$	—
13	$\text{H}^+ + \text{e}^- \rightarrow \text{H} + \gamma$	$k_{13,\text{A}} = 1.269 \times 10^{-13} \left(\frac{315614}{T}\right)^{1.503}$ $\times [1.0 + \left(\frac{604625}{T}\right)^{0.470}]^{-1.923}$ $k_{13,\text{B}} = 2.753 \times 10^{-14} \left(\frac{315614}{T}\right)^{1.500}$ $\times [1.0 + \left(\frac{115188}{T}\right)^{0.407}]^{-2.242}$	Case A 12 Case B 12
14	$\text{D}^+ + \text{e}^- \rightarrow \text{D} + \gamma$	$k_{14} = k_{13}$	—
15	$\text{H}^- + \text{e}^- \rightarrow \text{H} + \text{e}^- + \text{e}^-$	$k_{15} = \exp[-1.801849334 \times 10^1$	11

Table 1—Continued

No.	Reaction	Rate coefficient (cm ³ s ⁻¹)	Ref.	
		$+ 2.36085220 \times 10^0 \ln T_e$ $- 2.82744300 \times 10^{-1} (\ln T_e)^2$ $+ 1.62331664 \times 10^{-2} (\ln T_e)^3$ $- 3.36501203 \times 10^{-2} (\ln T_e)^4$ $+ 1.17832978 \times 10^{-2} (\ln T_e)^5$ $- 1.65619470 \times 10^{-3} (\ln T_e)^6$ $+ 1.06827520 \times 10^{-4} (\ln T_e)^7$ $- 2.63128581 \times 10^{-6} (\ln T_e)^8]$		
16	$\text{H}^- + \text{H} \rightarrow \text{H} + \text{H} + \text{e}^-$	$k_{16} = 2.5634 \times 10^{-9} T_e^{1.78186}$ $= \exp[-2.0372609 \times 10^1$ $+ 1.13944933 \times 10^0 \ln T_e$ $- 1.4210135 \times 10^{-1} (\ln T_e)^2$ $+ 8.4644554 \times 10^{-3} (\ln T_e)^3$ $- 1.4327641 \times 10^{-3} (\ln T_e)^4$ $+ 2.0122503 \times 10^{-4} (\ln T_e)^5$ $+ 8.6639632 \times 10^{-5} (\ln T_e)^6$ $- 2.5850097 \times 10^{-5} (\ln T_e)^7$ $+ 2.4555012 \times 10^{-6} (\ln T_e)^8$ $- 8.0683825 \times 10^{-8} (\ln T_e)^9]$	$T_e \leq 0.1 \text{ eV}$ $T_e > 0.1 \text{ eV}$	11
17	$\text{H}^- + \text{H}^+ \rightarrow \text{H}_2^+ + \text{e}^-$	$k_{17} = 6.9 \times 10^{-9} T^{-0.35}$ $= 9.6 \times 10^{-7} T^{-0.90}$	$T \leq 8000 \text{ K}$ $T > 8000 \text{ K}$	13
18	$\text{H} + \text{D}^+ \rightarrow \text{D} + \text{H}^+$	$k_{18} = 2.06 \times 10^{-10} T^{0.396} \exp\left(-\frac{33}{T}\right)$ $+ 2.03 \times 10^{-9} T^{-0.332}$		14
19	$\text{D} + \text{H}^+ \rightarrow \text{H} + \text{D}^+$	$k_{19} = 2.0 \times 10^{-10} T^{0.402} \exp\left(-\frac{37.1}{T}\right)$ $- 3.31 \times 10^{-17} T^{1.48}$ $= 3.44 \times 10^{-10} T^{0.35}$	$T \leq 2 \times 10^5 \text{ K}$ $T > 2 \times 10^5 \text{ K}$	14

Table 1—Continued

No.	Reaction	Rate coefficient ($\text{cm}^3 \text{s}^{-1}$)	Ref.
20	$\text{H}_2 + \text{D}^+ \rightarrow \text{HD} + \text{H}^+$	$k_{20} = [0.417 + 0.864 \log T - 0.137(\log T)^2] \times 10^{-9}$	15
21	$\text{HD} + \text{H}^+ \rightarrow \text{H}_2 + \text{D}^+$	$k_{21} = 1.1 \times 10^{-9} \exp\left(-\frac{488}{T}\right)$	15
22	$\text{H}_2 + \text{D} \rightarrow \text{HD} + \text{H}$	$k_{22} = 1.69 \times 10^{-10} \exp\left(-\frac{4680}{T}\right)$ $T \leq 200 \text{ K}$ $= 1.69 \times 10^{-10} \exp\left(-\frac{4680}{T} + \frac{198800}{T^2}\right)$ $T > 200 \text{ K}$	16
23	$\text{HD} + \text{H} \rightarrow \text{D} + \text{H}_2$	$k_{23} = 5.25 \times 10^{-11} \exp\left(-\frac{4430}{T}\right)$ $T \leq 200 \text{ K}$ $= 5.25 \times 10^{-11} \exp\left(-\frac{4430}{T} + \frac{173900}{T^2}\right)$ $T > 200 \text{ K}$	17
24	$\text{He} + \text{e}^- \rightarrow \text{He}^+ + \text{e}^- + \text{e}^-$	$k_{24} = \exp[-4.409864886 \times 10^1$ $+ 2.391596563 \times 10^1 \ln T_e$ $- 1.07532302 \times 10^1 (\ln T_e)^2$ $+ 3.05803875 \times 10^0 (\ln T_e)^3$ $- 5.6851189 \times 10^{-1} (\ln T_e)^4$ $+ 6.79539123 \times 10^{-2} (\ln T_e)^5$ $- 5.0090561 \times 10^{-3} (\ln T_e)^6$ $+ 2.06723616 \times 10^{-4} (\ln T_e)^7$ $- 3.64916141 \times 10^{-6} (\ln T_e)^8]$	11
25	$\text{He}^+ + \text{e}^- \rightarrow \text{He} + \gamma$	$k_{25,\text{rr,A}} = 10^{-11} T^{-0.5} [12.72 - 1.615 \log T$ $- 0.3162(\log T)^2 + 0.0493(\log T)^3]$ Case A $k_{25,\text{rr,B}} = 10^{-11} T^{-0.5} [11.19 - 1.676 \log T$ $- 0.2852(\log T)^2 + 0.04433(\log T)^3]$ Case B $k_{25,\text{di}} = 1.9 \times 10^{-3} T^{-1.5} \exp\left(-\frac{473421}{T}\right)$ $\times [1.0 + 0.3 \exp\left(-\frac{94684}{T}\right)]$ 19	18 18

Table 1—Continued

No.	Reaction	Rate coefficient (cm ³ s ⁻¹)	Ref.
26	He ⁺ + H → He + H ⁺	$k_{26} = 1.25 \times 10^{-15} \left(\frac{T}{300}\right)^{0.25}$	20
27	He + H ⁺ → He ⁺ + H	$k_{27} = 1.26 \times 10^{-9} T^{-0.75} \exp\left(-\frac{127500}{T}\right)$ $= 4.0 \times 10^{-37} T^{4.74}$	$T \leq 10000$ K $T > 10000$ K 21
28	He ⁺ + D → He + D ⁺	$k_{28} = k_{26}$	—
29	He + D ⁺ → He ⁺ + D	$k_{29} = k_{27}$	—
30	C ⁺ + e ⁻ → C + γ	$k_{30} = 4.67 \times 10^{-12} \left(\frac{T}{300}\right)^{-0.6}$ $= 1.23 \times 10^{-17} \left(\frac{T}{300}\right)^{2.49} \exp\left(\frac{21845.6}{T}\right)$ $= 9.62 \times 10^{-8} \left(\frac{T}{300}\right)^{-1.37} \exp\left(\frac{-115786.2}{T}\right)$	$T \leq 7950$ K $7950 \text{ K} < T \leq 21140$ K $T > 21140$ K 22
31	Si ⁺ + e ⁻ → Si + γ	$k_{31} = 7.5 \times 10^{-12} \left(\frac{T}{300}\right)^{-0.55}$ $= 4.86 \times 10^{-12} \left(\frac{T}{300}\right)^{-0.32}$ $= 9.08 \times 10^{-14} \left(\frac{T}{300}\right)^{0.818}$	$T \leq 2000$ K $2000 \text{ K} < T \leq 10^4$ K $T > 10^4$ K 23
32	O ⁺ + e ⁻ → O + γ	$k_{32} = 1.30 \times 10^{-10} T^{-0.64}$ $= 1.41 \times 10^{-10} T^{-0.66} + 7.4 \times 10^{-4} T^{-1.5}$ $\times \exp\left(-\frac{175000}{T}\right) [1.0 + 0.062 \times \exp\left(-\frac{145000}{T}\right)]$	$T \leq 400$ K $T > 400$ K 24
33	C + e ⁻ → C ⁺ + e ⁻ + e ⁻	$k_{33} = 6.85 \times 10^{-8} (0.193 + u)^{-1} u^{0.25} e^{-u}$	$u = 11.26/T_e$ 25

Table 1—Continued

No.	Reaction	Rate coefficient (cm ³ s ⁻¹)	Ref.
34	$\text{Si} + \text{e}^- \rightarrow \text{Si}^+ + \text{e}^- + \text{e}^-$	$k_{34} = 1.88 \times 10^{-7} (1.0 + u^{0.5}) (0.376 + u)^{-1} u^{0.25} e^{-u}$	$u = 8.2/T_e$ 25
35	$\text{O} + \text{e}^- \rightarrow \text{O}^+ + \text{e}^- + \text{e}^-$	$k_{35} = 3.59 \times 10^{-8} (0.073 + u)^{-1} u^{0.34} e^{-u}$	$u = 13.6/T_e$ 25
36	$\text{O}^+ + \text{H} \rightarrow \text{O} + \text{H}^+$	$k_{36} = 4.99 \times 10^{-11} T^{0.405} + 7.54 \times 10^{-10} T^{-0.458}$	26
37	$\text{O} + \text{H}^+ \rightarrow \text{O}^+ + \text{H}$	$k_{37} = [1.08 \times 10^{-11} T^{0.517} + 4.00 \times 10^{-10} T^{0.00669}] \exp(-\frac{227}{T})$	27
38	$\text{O} + \text{He}^+ \rightarrow \text{O}^+ + \text{He}$	$k_{38} = 4.991 \times 10^{-15} \left(\frac{T}{10000}\right)^{0.3794} \exp\left(-\frac{T}{1121000}\right) + 2.780 \times 10^{-15} \left(\frac{T}{10000}\right)^{-0.2163} \exp\left(\frac{T}{815800}\right)$	28
39	$\text{C} + \text{H}^+ \rightarrow \text{C}^+ + \text{H}$	$k_{39} = 3.9 \times 10^{-16} T^{0.213}$	27
40	$\text{C}^+ + \text{H} \rightarrow \text{C} + \text{H}^+$	$k_{40} = 6.08 \times 10^{-14} \left(\frac{T}{10000}\right)^{1.96} \exp\left(-\frac{170000}{T}\right)$	27
41	$\text{C} + \text{He}^+ \rightarrow \text{C}^+ + \text{He}$	$k_{41} = 8.58 \times 10^{-17} T^{0.757}$ $= 3.25 \times 10^{-17} T^{0.968}$ $= 2.77 \times 10^{-19} T^{1.597}$	$T \leq 200 \text{ K}$ $200 < T \leq 2000 \text{ K}$ $T > 2000 \text{ K}$ 29
42	$\text{Si} + \text{H}^+ \rightarrow \text{Si}^+ + \text{H}$	$k_{42} = 5.88 \times 10^{-13} T^{0.848}$ $= 1.45 \times 10^{-13} T$	$T \leq 10^4 \text{ K}$ $T > 10^4 \text{ K}$ 30

Table 1—Continued

No.	Reaction	Rate coefficient ($\text{cm}^3 \text{s}^{-1}$)	Ref.
43	$\text{Si} + \text{He}^+ \rightarrow \text{Si}^+ + \text{He}$	$k_{43} = 3.3 \times 10^{-9}$	31
44	$\text{C}^+ + \text{Si} \rightarrow \text{C} + \text{Si}^+$	$k_{44} = 2.1 \times 10^{-9}$	31
45	$\text{Si}^+ + \text{H}^+ \rightarrow \text{Si}^{++} + \text{H}$	$k_{45} = 4.10 \times 10^{-10} \left(\frac{T}{10000}\right)^{0.24} \times \left[1.0 + 3.17 \exp\left(\frac{T}{2.39 \times 10^6}\right)\right] \exp\left(-\frac{3.178}{T_e}\right)$	30
46	$\text{Si}^{++} + \text{H} \rightarrow \text{Si}^+ + \text{H}^+$	$k_{46} = 1.23 \times 10^{-9} \left(\frac{T}{10000}\right)^{0.24} \times \left[1.0 + 3.17 \exp\left(\frac{T}{2.39 \times 10^6}\right)\right]$	30
47	$\text{Si}^{++} + \text{e}^- \rightarrow \text{Si}^+ + \gamma$	$k_{47,\text{rr}} = 1.75 \times 10^{-12} \left(\frac{T}{10000}\right)^{-0.6346}$	32
		$k_{47,\text{di}} = 2.2552 \times 10^{-11} T_e^{-1.5} \exp\left(-\frac{2.76}{T_e}\right) + 5.6058 \times 10^{-9} T_e^{-1.5} \exp\left(-\frac{10.13}{T_e}\right)$	33

References. — 1: Wishart (1979), 2: Launay et al. (1991), 3: Ramaker & Peek (1976), 4: Karpas, Anicich & Huntress (1979), 5: Moseley et al. (1970), 6: Schneider et al. (1994), 7: Savin et al. (2004), 8: Stibbe & Tennyson (1999), 9: Mac Low & Shull (1986), 10: Martin, Keogh & Mandy (1998), 11: Janev et al. (1987), 12: Ferland et al. (1992), 13: Poulaert et al. (1978), 14: Savin (2002), 15: Gerlich (1982), 16: Mielke et al. (1994), 17: Shavitt (1959), 18: Hummer & Storey (1998), 19: Aldrovandi & Pequignot (1973), 20: Zygelman *et al.* (1989), 21: Kimura et al. (1993), 22: Nahar & Pradhan (1997), 23: Nahar (2000), 24: Nahar (1999), 25: Voronov (1997), 26: Stancil et al. (1999), 27: Stancil et al. (1998), 28: Zhao *et al.* (2004), 29: Kimura et al. (1993), 30: Kingdon & Ferland (1996), 31: Le Teuff, Millar & Markwick (2000), 32: Nahar (1995, 1996), 33: Mazzotta et al. (1998)

Note. — T and T_e are the gas temperature in units of K and eV respectively. References are to the primary source of data for each reaction.

Table 2. List of the photochemical gas-phase reactions in our chemical model.

No.	Reaction	Cross-section (cm ⁻²)		Reference
48	$\text{H} + \gamma \rightarrow \text{H}^+ + \text{e}^-$	$\sigma_{48} = 6.3 \times 10^{-18} \left(\frac{E_{\text{th}}}{E}\right)^4 \exp(4 - 4\varepsilon^{-1} \arctan \varepsilon) \times [1 - \exp(-2\pi/\varepsilon)]^{-1}$	$E_{\text{th}} = 13.6 \text{ eV}$ $\varepsilon = \sqrt{\frac{E}{13.6} - 1}$	1
49	$\text{D} + \gamma \rightarrow \text{D}^+ + \text{e}^-$	$\sigma_{49} = \sigma_{48}$	$E_{\text{th}} = 13.6 \text{ eV}$	1
50	$\text{He} + \gamma \rightarrow \text{He}^+ + \text{e}^-$	$\sigma_{50} = 3.1451 \times 10^{-16} \left(\frac{E_{\text{th}}}{E}\right)^{7/2} \times \left[1.0 - 4.7416 \left(\frac{E_{\text{th}}}{E}\right)^{1/2} + 14.82 \left(\frac{E_{\text{th}}}{E}\right) - 30.8678 \left(\frac{E_{\text{th}}}{E}\right)^{3/2} + 37.3584 \left(\frac{E_{\text{th}}}{E}\right)^2 - 23.4585 \left(\frac{E_{\text{th}}}{E}\right)^{5/2} + 5.9133 \left(\frac{E_{\text{th}}}{E}\right)^3\right]$	$E_{\text{th}} = 24.6 \text{ eV}$	2
51	$\text{H}^- + \gamma \rightarrow \text{H} + \text{e}^-$	$\sigma_{51} = 2.11 \times 10^{-16} (E - E_{\text{th}})^{3/2} E^{-3}$	$E_{\text{th}} = 0.755 \text{ eV}$	3
52	$\text{H}_2^+ + \gamma \rightarrow \text{H} + \text{H}^+$	$\sigma_{52} = \text{dex} \left[-40.97 + 15.9795 \left(\frac{E}{E_{\text{th}}}\right) - 3.53934 \left(\frac{E}{E_{\text{th}}}\right)^2 + 0.2581155 \left(\frac{E}{E_{\text{th}}}\right)^3 \right]$ $= \text{dex} \left[-30.26 + 7.3935 \left(\frac{E}{E_{\text{th}}}\right) - 1.29214 \left(\frac{E}{E_{\text{th}}}\right)^2 + 6.5785 \times 10^{-2} \left(\frac{E}{E_{\text{th}}}\right)^3 \right]$	$E_{\text{th}} = 2.65 \text{ eV}$ $2.65 < E < 11.27 \text{ eV}$ $11.27 < E < 21.0 \text{ eV}$	4
53	$\text{H}_2 + \gamma \rightarrow \text{H} + \text{H}$	See §2.4.1		5
54	$\text{H}_2 + \gamma \rightarrow \text{H}_2^+ + \text{e}^-$	$\sigma_{54} = 9.548 \times 10^{-17} \left(\frac{E}{E_{\text{th}}}\right) - 9.4 \times 10^{-17}$ $= 2.16 \times 10^{-17} \left(\frac{E}{E_{\text{th}}}\right) - 1.48 \times 10^{-17}$ $= 1.51 \times 10^{-17} \left(\frac{E}{E_{\text{th}}}\right)^{2.71}$	$E_{\text{th}} = 15.4 \text{ eV}$ $15.4 < E < 16.5 \text{ eV}$ $16.5 < E < 17.7 \text{ eV}$ $17.7 < E < 30.0 \text{ eV}$	6
55	$\text{HD} + \gamma \rightarrow \text{H} + \text{D}$	See §2.4.1		7
56	$\text{C} + \gamma \rightarrow \text{C}^+ + \text{e}^-$	$\sigma_{56} = 5.027 \times 10^{-16} F(x, y, y_w, y_a, P)$	$E_{\text{th}} = 11.26 \text{ eV}$ $x = \frac{E}{2.144} - 1.133$ $y = \sqrt{x^2 + 1.607^2}$ $y_w = 0.09157$ $y_a = 62.16$ $P = 5.101$	8
57	$\text{O} + \gamma \rightarrow \text{O}^+ + \text{e}^-$	$\sigma_{57} = 1.745 \times 10^{-15} F(x, y, y_w, y_a, P)$	$E_{\text{th}} = 13.62 \text{ eV}$	8

Table 2—Continued

No.	Reaction	Cross-section (cm ⁻²)	Reference
		$x = \frac{E}{1.240} - 8.698$ $y = \sqrt{x^2 + 0.1271^2}$ $y_w = 0.07589$ $y_a = 3.784$ $P = 17.64$	
58	Si + $\gamma \rightarrow \text{Si}^+ + \text{e}^-$	$\sigma_{58} = 2.506 \times 10^{-17} F(x, y, y_w, y_a, P)$	8
		$E_{\text{th}} = 8.152 \text{ eV}$ $x = \frac{E}{23.17} - 1.672 \times 10^{-5}$ $y = \sqrt{x^2 + 0.4207^2}$ $y_w = 0.2837$ $y_a = 20.57$ $P = 3.546$	
59	Si ⁺ + $\gamma \rightarrow \text{Si}^{++} + \text{e}^-$	$\sigma_{59} = 4.140 \times 10^{-18} F(x, y, y_w, y_a, P)$	8
		$E_{\text{th}} = 16.35 \text{ eV}$ $x = \frac{E}{2.556} - 6.634$ $y = \sqrt{x^2 + 0.1272^2}$ $y_w = 1.570$ $y_a = 13.37$ $P = 11.91$	

References. — 1: Osterbrock (1989), 2: Yan, Sadeghpour & Dalgarno (1998), 3: de Jong (1972); Shapiro & Kang (1987), 4: Dunn (1968), 5: Draine & Bertoldi (1996), 6: O’Neil & Reinhardt (1978); Wilms, Allen & McCray (2002), 7: Abgrall & Roueff (2006), 8: Verner et al. (1996)

Note. — References are to the primary source of data for each reaction. E is the photon energy in eV and E_{th} is the energy threshold in eV. The fitting function F used in the tabulated cross-sections for reactions 55–58 is from Verner et al. (1996) and is given by $F = [(x - 1)^2 + y_w^2] y^{0.5P - 5.5} (1 + \sqrt{y/y_a})^{-P}$. Photodissociation of H₂ and HD occurs via absorption into a large number of discrete spectral lines and so no simple cross-section can be given for these processes; see §2.4.1 for more details

Table 3. List of the grain surface reactions included in our chemical model.

No.	Reaction	Rate coefficient ($\text{cm}^3 \text{s}^{-1}$)	Ref.
60	$\text{H} + \text{H} \rightarrow \text{H}_2$	$k_{60} = 3.0 \times 10^{-18} T^{0.5} (\mathcal{D}/\mathcal{D}_\odot) [1.0 + 4 \times 10^{-2} (T + T_{\text{gr}})^{0.5} + 2 \times 10^{-3} T + 8 \times 10^{-6} T^2]^{-1} \left[1.0 + 10^4 \exp\left(-\frac{600}{T_{\text{gr}}}\right) \right]^{-1}$	1
61	$\text{H}^+ + \text{e}^- \rightarrow \text{H}$	$k_{61} = 1.225 \times 10^{-13} (\mathcal{D}/\mathcal{D}_\odot) [1.0 + 8.074 \times 10^{-6} \psi^{1.378} (1.0 + 5.087 \times 10^2 T^{0.01586} \psi^{-0.4723 - 1.102 \times 10^{-5} \ln T})]^{-1}$	2
62	$\text{D}^+ + \text{e}^- \rightarrow \text{D}$	$k_{62} = \frac{1}{\sqrt{2}} k_{61}$	3
63	$\text{He}^+ + \text{e}^- \rightarrow \text{He}$	$k_{63} = 5.572 \times 10^{-14} (\mathcal{D}/\mathcal{D}_\odot) [1.0 + 3.185 \times 10^{-7} \psi^{1.512} (1.0 + 5.115 \times 10^3 T^{3.903 \times 10^{-7}} \psi^{-0.4956 - 5.494 \times 10^{-7} \ln T})]^{-1}$	2
64	$\text{C}^+ + \text{e}^- \rightarrow \text{C}$	$k_{64} = 4.558 \times 10^{-13} (\mathcal{D}/\mathcal{D}_\odot) [1.0 + 6.089 \times 10^{-3} \psi^{1.128} (1.0 + 4.331 \times 10^2 T^{0.04845} \psi^{-0.8120 - 1.333 \times 10^{-4} \ln T})]^{-1}$	2
65	$\text{O}^+ + \text{e}^- \rightarrow \text{O}$	$k_{65} = \frac{1}{4} k_{61}$	3
66	$\text{Si}^+ + \text{e}^- \rightarrow \text{Si}$	$k_{66} = 2.166 \times 10^{-14} (\mathcal{D}/\mathcal{D}_\odot) [1.0 + 5.678 \times 10^{-8} \psi^{1.874} (1.0 + 4.375 \times 10^4 T^{1.635 \times 10^{-6}} \psi^{-0.8964 - 7.538 \times 10^{-5} \ln T})]^{-1}$	2

Note. — \mathcal{D} is the dust-to-gas ratio and \mathcal{D}_\odot is the dust-to-gas ratio in the local ISM. We generally assume that $\mathcal{D}/\mathcal{D}_\odot \equiv Z/Z_\odot$. T and T_{gr} are the gas and grain temperatures, respectively. The parameter ψ in the grain recombination rates is given by $\psi = G\sqrt{T}/n_e$, where $G \simeq 0.01 J_{21}$ is a measure of the radiation energy density between 6 eV and 13.6 eV relative to the Habing (1968) field.

References. — 1: Hollenbach & McKee (1979); 2: Weingartner & Draine (2001a); 3: This work, but based on Weingartner & Draine (2001a)

Table 4. List of cosmic ray ionization processes included in our chemical model

No.	Reaction	ζ_i/ζ_H	Ref.
67	$H + \text{c.r.} \rightarrow H^+ + e^-$	1.0	Le Teuff, Millar & Markwick (2000)
68	$D + \text{c.r.} \rightarrow D^+ + e^-$	1.0	Le Teuff, Millar & Markwick (2000)
69	$\text{He} + \text{c.r.} \rightarrow \text{He}^+ + e^-$	1.09	Le Teuff, Millar & Markwick (2000)
70	$\text{H}_2 + \text{c.r.} \rightarrow \text{H}_2^+ + e^-$	2.0	Le Teuff, Millar & Markwick (2000)
71	$\text{C} + \text{c.r.} \rightarrow \text{C}^+ + e^-$	3.83	Le Teuff, Millar & Markwick (2000)
72	$\text{O} + \text{c.r.} \rightarrow \text{O}^+ + e^-$	5.67	Le Teuff, Millar & Markwick (2000)
73	$\text{Si} + \text{c.r.} \rightarrow \text{Si}^+ + e^-$	6.5	Lotz (1967); Langer (1978)
74	$\text{Si}^+ + \text{c.r.} \rightarrow \text{Si}^{++} + e^-$	2.5	Lotz (1967); Langer (1978)

Note. — We list here the ratio of the various rates to the rate of process 67, the cosmic ray ionization of atomic hydrogen, ζ_H , which we treat as an adjustable parameter in our models. Rates for cosmic ray ionization of Si and Si^+ were calculated following the prescription in Langer (1978) and using data from Lotz (1967) under the assumption that the effective number of outer shell electrons for Si and Si^+ in the high energy limit is the same as that for C and C^+ .

Table 5. Atomic data for the fine structure transitions included in our thermal model

Coolant	Transition	g_j	g_i	$\lambda_{ji}(\mu\text{m})$	E_{ji}/k (K)	A_{ji} (s^{-1})
C	$1 \rightarrow 0$	3	1	609.2	24	7.9×10^{-8}
C	$2 \rightarrow 0$	5	1	229.9	63	2.1×10^{-14}
C	$2 \rightarrow 1$	5	3	369.0	39	2.7×10^{-7}
O	$1 \rightarrow 0$	3	5	63.1	230	8.9×10^{-5}
O	$2 \rightarrow 0$	1	5	44.2	330	1.3×10^{-10}
O	$2 \rightarrow 1$	1	3	145.6	98	1.8×10^{-5}
Si	$1 \rightarrow 0$	3	1	129.6	110	8.4×10^{-6}
Si	$2 \rightarrow 0$	5	1	44.8	320	2.4×10^{-10}
Si	$2 \rightarrow 1$	5	3	68.4	210	4.2×10^{-5}
C ⁺	$1 \rightarrow 0$	4	2	157.7	92	2.3×10^{-6}
Si ⁺	$1 \rightarrow 0$	4	2	34.8	410	2.2×10^{-4}

Table 6. Collisional de-excitation rates for atomic fine-structure coolants

Coolant	Collider	De-excitation rates ($\text{cm}^3 \text{s}^{-1}$)	Temperature range	Refs.
C	o-H ₂	$q_{10} = 8.7 \times 10^{-11} - 6.6 \times 10^{-11} \exp\left(-\frac{T}{218.3}\right)$		1
		$+ 6.6 \times 10^{-11} \exp\left(-\frac{2T}{218.3}\right)$		1
		$q_{20} = 1.2 \times 10^{-10} - 6.1 \times 10^{-11} \exp\left(-\frac{T}{387.3}\right)$		1
		$q_{21} = 2.9 \times 10^{-10} - 1.9 \times 10^{-10} \exp\left(-\frac{T}{348.9}\right)$		1
C	p-H ₂	$q_{10} = 7.9 \times 10^{-11} - 8.7 \times 10^{-11} \exp\left(-\frac{T}{126.4}\right)$		1
		$+ 1.3 \times 10^{-10} \exp\left(-\frac{2T}{126.4}\right)$		1
		$q_{20} = 1.1 \times 10^{-10} - 8.6 \times 10^{-11} \exp\left(-\frac{T}{223.0}\right)$		1
		$+ 8.7 \times 10^{-11} \exp\left(-\frac{2T}{223.0}\right)$		1
		$q_{21} = 2.7 \times 10^{-10} - 2.6 \times 10^{-10} \exp\left(-\frac{T}{250.7}\right)$		1
C	H	$q_{10} = 1.6 \times 10^{-10} T_2^{0.14}$		2
		$q_{20} = 9.2 \times 10^{-11} T_2^{0.26}$		2
		$q_{21} = 2.9 \times 10^{-10} T_2^{0.26}$		2
C	H ⁺	$q_{10} = (9.6 \times 10^{-11} - 1.8 \times 10^{-14} T + 1.9 \times 10^{-18} T^2) T^{0.45}$	$T \leq 5000 \text{ K}$	3
		$= 8.9 \times 10^{-10} T^{0.117}$	$T > 5000 \text{ K}$	3
		$q_{20} = (3.1 \times 10^{-12} - 6.0 \times 10^{-16} T + 3.9 \times 10^{-20} T^2) T$	$T \leq 5000 \text{ K}$	3
		$= 2.3 \times 10^{-9} T^{0.0965}$	$T > 5000 \text{ K}$	3
		$q_{21} = (1.0 \times 10^{-10} - 2.2 \times 10^{-14} T + 1.7 \times 10^{-18} T^2) T^{0.70}$	$T \leq 5000 \text{ K}$	3
		$= 9.2 \times 10^{-9} T^{0.0535}$	$T > 5000 \text{ K}$	3
C	e ⁻	$q_{10} = 2.88 \times 10^{-6} T^{-0.5} \exp[-9.25141 - 7.73782 \times 10^{-1} \ln T$		
		$+ 3.61184 \times 10^{-1} (\ln T)^2 - 1.50892 \times 10^{-2} (\ln T)^3$		
		$- 6.56325 \times 10^{-3} (\ln T)^4]$	$T \leq 10^3 \text{ K}$	4
		$= 2.88 \times 10^{-6} T^{-0.5} \exp[-4.44600 \times 10^2 - 2.27913 \times 10^2 \ln T$		
		$+ 4.2595 \times 10^1 (\ln T)^2 - 3.47620 \times 10^{-0} (\ln T)^3$		
		$+ 1.0508 \times 10^{-1} (\ln T)^4]$	$T > 10^3 \text{ K}$	4
C	e ⁻	$q_{20} = 1.73 \times 10^{-6} T^{-0.5} \exp[-7.69735 - 1.30743 \ln T$		
		$+ 0.697638 (\ln T)^2 - 0.111338 (\ln T)^3]$		

Table 6—Continued

Coolant	Collider	De-excitation rates (cm ³ s ⁻¹)	Temperature range	Refs.
		$+ 0.705277 \times 10^{-2}(\ln T)^4]$	$T \leq 10^3$ K	4
		$= 1.73 \times 10^{-6}T^{-0.5} \exp[3.50609 \times 10^2 - 1.87474 \times 10^2 \ln T$ $+ 3.61803 \times 10^1(\ln T)^2 - 3.03283 \times 10^0(\ln T)^3$ $+ 9.38138 \times 10^{-2}(\ln T)^4]$	$T > 10^3$ K	4
		$q_{21} = 1.73 \times 10^{-6}T^{-0.5} \exp[-7.4387 - 0.57443 \ln T$ $+ 0.358264(\ln T)^2 - 4.18166 \times 10^{-2}(\ln T)^3$ $+ 2.35272 \times 10^{-3}(\ln T)^4]$	$T \leq 10^3$ K	4
		$= 1.73 \times 10^{-6}T^{-0.5} \exp[3.86186 \times 10^2 - 2.02192 \times 10^2 \ln T$ $+ 3.85049 \times 10^1(\ln T)^2 - 3.19268 \times 10^0(\ln T)^3$ $+ 9.78573 \times 10^{-2}(\ln T)^4]$	$T > 10^3$ K	4
O	o-H ₂	$q_{10} = 2.7 \times 10^{-11}T^{0.362}$ $q_{20} = 5.49 \times 10^{-11}T^{0.317}$ $q_{21} = 2.74 \times 10^{-14}T^{1.060}$		5 5 5
O	p-H ₂	$q_{10} = 3.46 \times 10^{-11}T^{0.316}$ $q_{20} = 7.07 \times 10^{-11}T^{0.268}$ $q_{21} = 3.33 \times 10^{-15}T^{1.360}$		5 5 5
O	H	$q_{10} = 9.2 \times 10^{-11}T_2^{0.67}$ $q_{20} = 4.3 \times 10^{-11}T_2^{0.80}$ $q_{21} = 1.1 \times 10^{-10}T_2^{0.44}$		5 5 5
O	H ⁺	$q_{10} = \begin{cases} 6.38 \times 10^{-11}T^{0.40} & T \leq 194 \text{ K} \\ 7.75 \times 10^{-12}T^{0.80} & 194 < T \leq 3686 \text{ K} \\ 2.65 \times 10^{-10}T^{0.37} & T > 3686 \text{ K} \end{cases}$		6
		$q_{20} = \begin{cases} 6.10 \times 10^{-13}T^{1.10} & T \leq 511 \text{ K} \\ 2.12 \times 10^{-12}T^{0.90} & 511 < T \leq 7510 \text{ K} \\ 4.49 \times 10^{-10}T^{0.30} & T > 7510 \text{ K} \end{cases}$		6
		$q_{21} = \begin{cases} 2.03 \times 10^{-11}T^{0.56} & T \leq 2090 \text{ K} \\ 3.43 \times 10^{-10}T^{0.19} & T > 2090 \text{ K} \end{cases}$		6
O	e ⁻	$q_{10} = 5.12 \times 10^{-10}T^{-0.075}$ $q_{20} = 4.86 \times 10^{-10}T^{-0.026}$ $q_{21} = 1.08 \times 10^{-14}T^{0.926}$		7 7 7

Table 6—Continued

Coolant	Collider	De-excitation rates (cm ³ s ⁻¹)	Temperature range	Refs.
Si	H	$q_{10} = 3.5 \times 10^{-10} T_2^{-0.03}$		2
		$q_{20} = 1.7 \times 10^{-11} T_2^{0.17}$		2
		$q_{21} = 5.0 \times 10^{-10} T_2^{0.17}$		2
Si	H ⁺	$q_{10} = 7.2 \times 10^{-9}$		2
		$q_{20} = 7.2 \times 10^{-9}$		2
		$q_{21} = 2.2 \times 10^{-8}$		2
C ⁺	o-H ₂	$q_{10} = \begin{cases} 4.7 \times 10^{-10} + 4.6 \times 10^{-13} T & T \leq 250 \text{ K} \\ 5.85 \times 10^{-10} T^{0.07} & T > 250 \text{ K} \end{cases}$		8, 9
C ⁺	p-H ₂	$q_{10} = \begin{cases} 2.5 \times 10^{-10} T^{0.12} & T \leq 250 \text{ K} \\ 4.85 \times 10^{-10} T^{0.07} & T > 250 \text{ K} \end{cases}$		8, 9
C ⁺	H	$q_{10} = \begin{cases} 8.0 \times 10^{-10} T_2^{0.07} & T \leq 2000 \text{ K} \\ 3.1 \times 10^{-10} T_2^{0.385} & T > 2000 \text{ K} \end{cases}$		2, 10
C ⁺	e ⁻	$q_{10} = \begin{cases} 3.86 \times 10^{-7} T_2^{-0.5} & T \leq 2000 \text{ K} \\ 2.43 \times 10^{-7} T_2^{-0.345} & T > 2000 \text{ K} \end{cases}$		11
Si ⁺	H	$q_{10} = 4.95 \times 10^{-10} T_2^{0.24}$		12
Si ⁺	e ⁻	$q_{10} = 1.2 \times 10^{-6} T_2^{-0.5}$		13

Note. — o-H₂ and p-H₂ denote ortho-H₂ and para-H₂ respectively. T is the gas temperature (in Kelvin) and $T_2 = 10^{-2}T$.

References. — 1: Schroder et al. (1991); 2: Hollenbach & McKee (1989); 3: Roueff & Le Bourlot (1990); 4: Johnson et al. (1987); 5: Flower, private communication; 6: Pequignot (1990, 1996); 7: Bell, Berrington & Thomas (1998); 8: Flower & Launay (1977); 9: assumed to have the same scaling with T as the low temperature H rate for temperatures above the range of the Flower & Launay (1977) fit; 10: Keenan *et al.* (1986); 11: Wilson & Bell (2002); 12: Roueff (1990); 13: Dufton & Kingston (1991), extrapolated to $T < 4000$ K assuming constant collision strength

Table 7. Other processes included in our thermal model.

Process	Rate (erg cm ⁻³ s ⁻¹)	Ref.
Cooling:		
H excitation	$\Lambda = 7.5 \times 10^{-19} \left(1.0 + \sqrt{T/10^5}\right)^{-1} \exp\left(-\frac{118348}{T}\right) n_e n_H$	1
He excitation (1 ¹ S state)	$\Lambda = 1.1 \times 10^{-19} T^{0.082} \exp\left(-\frac{230000}{T}\right) n_e n_{\text{He}}$	2
He excitation (2 ³ S state)	$\Lambda = 9.1 \times 10^{-27} T^{-0.1687} \left(1.0 + \sqrt{T/10^5}\right)^{-1} \exp\left(-\frac{473638}{T}\right) n_e^2 n_{\text{He}^+}$	1
He ⁺ excitation	$\Lambda = 5.54 \times 10^{-17} T^{-0.397} \left(1.0 + \sqrt{T/10^5}\right)^{-1} \exp\left(-\frac{118348}{T}\right) n_e n_{\text{He}^+}$	1
H collisional ionization	$\Lambda = 2.179 \times 10^{-11} k_{11} n_e n_H$	3
He collisional ionization	$\Lambda = 3.94 \times 10^{-11} k_{24} n_e n_{\text{He}}$	3
Compton cooling	$\Lambda = 1.017 \times 10^{-37} T_{\text{CMB}}^4 (T - T_{\text{CMB}}) n_e$	1
Bremsstrahlung	$\Lambda = 1.426 \times 10^{-27} Z_i^2 T^{1/2} g_{\text{ff}}(Z_i, T) n_e n_i$ $g_{\text{ff}} = 0.79464 + 0.1243 \log(T/Z_i^2) \quad (T/Z_i^2) < 320000 \text{ K}$ $\quad = 2.13164 - 0.1240 \log(T/Z_i^2) \quad (T/Z_i^2) > 320000 \text{ K}$	4
H ⁺ recombination (radiative)	$\Lambda = 1.38 \times 10^{-16} T k_{13} n_e n_{\text{H}^+}$	5
He ⁺ recombination (radiative)	$\Lambda = 1.38 \times 10^{-16} T k_{25,\text{rr}} n_e n_{\text{He}^+}$	6
He ⁺ recombination (dielectronic)	$\Lambda = 6.54 \times 10^{-11} k_{25,\text{di}} n_e n_{\text{He}^+}$	7
Grain surface recombination	$\Lambda = 2.33 \times 10^{-30} T^{0.94} \tilde{\psi}^{0.74/T^{0.068}} \left(\frac{Z}{Z_{\odot}}\right) n_e n$	8
H ₂ rovibrational lines	See §3.2	9
HD rovibrational lines	See §3.2	10

Table 7—Continued

Process	Rate (erg cm ⁻³ s ⁻¹)	Ref.
H ₂ collisional dissociation	$\Lambda = 7.2 \times 10^{-12} (k_9 n_{\text{H}} + k_{10} n_{\text{H}_2}) n_{\text{H}_2}$	11
Gas-grain energy transfer	$\Lambda = 3.8 \times 10^{-33} T^{1/2} (T - T_{\text{gr}}) [1.0 - 0.8 \exp(-\frac{75}{T})] \left(\frac{Z}{Z_{\odot}}\right) n^2$	12
Heating:		
Photoelectric effect	$\Gamma = 1.3 \times 10^{-24} \epsilon G \left(\frac{Z}{Z_{\odot}}\right) n$ $\epsilon = \frac{4.9 \times 10^{-2}}{1.0 + 4.0 \times 10^{-3} \psi^{0.73}} + \frac{3.7 \times 10^{-2} (T/10000)^{0.7}}{1.0 + 2.0 \times 10^{-4} \psi}$	13
H ₂ photodissociation	$\Gamma = 6.4 \times 10^{-13} R_{\text{diss}} n_{\text{H}_2}$	14
UV pumping of H ₂	$\Gamma = 2.7 \times 10^{-11} R_{\text{diss}} n_{\text{H}_2} \left(\frac{n}{n+n_{\text{cr}}}\right)$	15
H photoionization	Dependent on incident spectrum; see §2.4	16
He photoionization	Dependent on incident spectrum; see §2.4	17
Gas-phase H ₂ formation	$\Gamma = \left[2.93 \times 10^{-12} k_2 n_{\text{H}^-} + 5.65 \times 10^{-12} k_4 n_{\text{H}_2^+}\right] n_{\text{H}} \left(\frac{n}{n+n_{\text{cr}}}\right)$	18
H ₂ formation on dust grains	$\Gamma = 7.16 \times 10^{-12} k_{60} n n_{\text{H}} \left(\frac{n}{n+n_{\text{cr}}}\right)$	19
Cosmic-ray ionization	$\Gamma = 3.2 \times 10^{-11} \zeta_{\text{tot}} n$	20

References. — 1: Cen (1992), 2: Bray et al. (2000), 3: Janev et al. (1987), 4: Shapiro & Kang (1987) 5: Ferland et al. (1992), 6: Hummer & Storey (1998), 7: Aldrovandi & Pequignot (1973), 8: Wolfire *et al.* (2003), 9: Le Bourlot et al. (1999), 10: Lipovka, Núñez-López, & Avila-Reese (2005), 11: Mac Low & Shull (1986); Martin, Keogh & Mandy (1998), 12: Hollenbach & McKee (1989), 13: Bakes & Tielens (1994); Wolfire *et al.* (1995), 14: Black & Dalgarno (1977), 15: Burton et al. (1990), 16: Osterbrock (1989), 17: Yan, Sadeghpour & Dalgarno (1998), 18: Launay et al. (1991);

Karpas, Anicich & Huntress (1979), 19: Hollenbach & McKee (1979), 20: Goldsmith & Langer (1978)

Note. — Z_i and n_i are the ion charge and number density of ion i . The parameter $\tilde{\psi}$ is given by $\tilde{\psi} = G\sqrt{T}/0.5n_e$, where $G \simeq 0.01J_{21}$ is a measure of the radiation energy density between 6 eV and 13.6 eV relative to the Habing (1968) field. R_{diss} is the photodissociation rate, calculated as discussed in §2.4.1. ζ_{tot} is the total cosmic-ray ionization rate (i.e. the sum of the rates for the various different species, weighted by their fractional abundances: $\zeta_{\text{tot}} = \sum_i x_i \zeta_i$). Finally, note that our treatment of recombination cooling here is approximate, but that it should be accurate enough for most purposes.